

# A Statistical Study of the Solar Wind Dependence of Multi-Harmonic Toroidal ULF Waves Observed by the Arase Satellite

著者	Yamamoto K., Seki K., Matsuoka A., Imajo S., Teramoto M., Kitahara M., Kasahara Y., Kumamoto A., Tsuchiya F., Shoji M., Nakamura S., Miyoshi Y., Shinohara I.
journal or publication title	Journal of Geophysical Research: Space Physics
volume	127
number	1
page range	e2021JA029840-1-e2021JA029840-17
year	2021-12-28
URL	<a href="http://hdl.handle.net/10228/00009053">http://hdl.handle.net/10228/00009053</a>

doi: <https://doi.org/10.1029/2021JA029840>

# JGR Space Physics

## RESEARCH ARTICLE

10.1029/2021JA029840

### Special Section:

Geospace multi-point observations in Van Allen Probes and Arase era

### Key Points:

- We statistically study solar wind dependence of multi-harmonic toroidal ultra-low frequency waves observed by the Arase satellite for ~3.5 years
- Solar wind velocity, dynamic pressure fluctuations, cone angle, and local plasma density affect the activity of the multi-harmonic waves
- The Kelvin Helmholtz instability drives the multi-harmonic waves at flanks while the waves around noon are related to upstream waves

### Correspondence to:

K. Yamamoto,  
yamamoto.kazuhiro@eps.s.u-tokyo.ac.jp

### Citation:

Yamamoto, K., Seki, K., Matsuoka, A., Imajo, S., Teramoto, M., Kitahara, M., et al. (2022). A Statistical study of the solar wind dependence of multi-harmonic toroidal ULF waves observed by the Arase satellite. *Journal of Geophysical Research: Space Physics*, 127, e2021JA029840. <https://doi.org/10.1029/2021JA029840>

Received 1 AUG 2021

Accepted 19 DEC 2021

### Author Contributions:

**Conceptualization:** K. Yamamoto, K. Seki

**Data curation:** A. Matsuoka, S. Imajo, M. Teramoto, M. Kitahara, Y. Kasahara, A. Kumamoto, F. Tsuchiya, M. Shoji, S. Nakamura, Y. Miyoshi, I. Shinohara

**Formal analysis:** K. Yamamoto

**Funding acquisition:** K. Yamamoto

**Investigation:** K. Yamamoto

**Methodology:** K. Yamamoto, K. Seki














**Project Administration:** Y. Miyoshi, I. Shinohara

**Resources:** A. Matsuoka, S. Imajo, M. Teramoto, M. Kitahara, Y. Kasahara, A. Kumamoto, F. Tsuchiya, M. Shoji, S. Nakamura, Y. Miyoshi, I. Shinohara

**Software:** K. Yamamoto, S. Imajo

© 2021. American Geophysical Union.  
All Rights Reserved.

## A Statistical Study of the Solar Wind Dependence of Multi-Harmonic Toroidal ULF Waves Observed by the Arase Satellite

K. Yamamoto<sup>1</sup> , K. Seki<sup>1</sup> , A. Matsuoka<sup>2</sup> , S. Imajo<sup>2</sup> , M. Teramoto<sup>3</sup> , M. Kitahara<sup>4</sup> , Y. Kasahara<sup>5</sup> , A. Kumamoto<sup>6</sup> , F. Tsuchiya<sup>6</sup> , M. Shoji<sup>4</sup> , S. Nakamura<sup>4</sup> , Y. Miyoshi<sup>4</sup> , and I. Shinohara<sup>7</sup> 

<sup>1</sup>Graduate School of Science, The University of Tokyo, Tokyo, Japan, <sup>2</sup>Graduate School of Science, Kyoto University, Kyoto, Japan, <sup>3</sup>Graduate School of Engineering, Kyushu Institute of Technology, Kita-kyushu, Japan, <sup>4</sup>Institute for Space-Earth Environmental Research, Nagoya University, Nagoya, Japan, <sup>5</sup>Graduate School of Natural Science and Technology, Kanazawa University, Kanazawa, Japan, <sup>6</sup>Graduate School of Science, Tohoku University, Sendai, Japan, <sup>7</sup>Institute of Space and Astronautical Science, Japan Aerospace Exploration Agency, Sagami-hara, Japan

**Abstract** Toroidal standing Alfvén wave is one of the ultra-low frequency waves that are frequently observed in the terrestrial magnetosphere. They sometimes exhibit multi-harmonic frequency spectra, indicating wide energy range input in the magnetosphere. However, their energy source has not been fully understood due to the lack of statistical studies. Here we used the data of the Arase satellite observations for ~3.5 years and conducted a statistical analysis of the solar wind dependence of the occurrence rate, wave power, and frequency of the multi-harmonic toroidal waves. We automatically detected the multi-harmonic waves and categorized them into four groups according to the solar wind velocity and the cone angle of the interplanetary magnetic field. We found that the occurrence rate and wave power of the multi-harmonic waves increase with the solar wind velocity on the flank sides. In the noon sector, the occurrence rate of the multi-harmonic waves increases with the decrease of the cone angle. The median frequency of the multi-harmonic waves on the dayside is positively correlated with the upstream wave frequency predicted by the theory of the ion beam instability for a small cone angle. The occurrence rate also increases with the solar wind dynamic pressure fluctuations. Therefore, we suggest that the Kelvin-Helmholtz instability, the upstream waves, and the dynamic pressure fluctuations are possible sources of the multi-harmonic waves. This study sheds light on the activity of the multi-harmonic waves which can affect radiation belt electrons under various solar wind conditions.

## 1. Introduction

Ultralow frequency (ULF) waves, whose frequency range is within 1.67–100 mHz, can interact with charged particles coherently (Zong et al., 2007) or stochastically (Schulz & Lanerotti, 1974) through the drift/drift-bounce resonance. Their interaction has been investigated by numerous previous studies because the ULF waves can adiabatically accelerate charged particles (e.g., Claudepierre et al., 2013; Elkington et al., 1999; Fei et al., 2006; Kamiya et al., 2018; Kanekal & Miyoshi, 2021; Ozeke et al., 2014, 2012). Wave frequency is one of the parameters which determine the energy where the wave-particle interaction occurs as well as azimuthal wave number (Elkington et al., 1999; Southwood et al., 1969). For example, Pc 5 (1.67–6.7 mHz) waves can interact with relativistic electrons through drift resonance because the drift frequency of the relativistic electrons is in the Pc 5 frequency range (e.g., Tan et al., 2004; Teramoto et al., 2019). The condition of the drift resonance can be expressed as  $\omega - m\omega_d = 0$ , where  $\omega$  is the wave angular frequency,  $m$  is the azimuthal wave number ( $m$  number), and  $\omega_d$  is the drift angular frequency. Pc 5 waves driven by the solar wind have a low- $m$  number ( $m \lesssim 10$ ) (e.g., Olson & Rostoker, 1978; Ponomarenko et al., 2001; Sarris et al., 2013), and hence they can satisfy the condition of the drift resonance ( $\omega \sim m\omega_d$ ). As numerically simulated by Sarris et al. (2017), ULF waves with broadband frequencies can cause radial diffusion of relativistic electrons in a wider energy range than monochromatic waves. Therefore, the classification of ULF waves according to the broadness of their frequency spectra is helpful for us to accurately understand the wave-particle interaction and energy dynamics of the radiation belts in the terrestrial magnetosphere (Murphy et al., 2020; Sarris, 2014). Recently, Murphy et al. (2020) investigated the occurrence of the broadband and monochromatic ULF waves observed by the GOES-15 satellite and their dependence on the solar wind condition. Using the AFINO code (Inglis et al., 2015, 2016), they fitted the power spectral density of

**Supervision:** K. Seki  
**Validation:** K. Yamamoto  
**Visualization:** K. Yamamoto  
**Writing – original draft:** K. Yamamoto  
**Writing – review & editing:** K. Yamamoto, K. Seki, A. Matsuoka, S. Imajo, M. Teramoto, M. Kitahara, Y. Kasahara, A. Kumamoto, F. Tsuchiya, M. Shoji, S. Nakamura, Y. Miyoshi, I. Shinohara

the magnetic field with three model functions of frequency and automatically chose the most reasonable model among them by Bayesian information criterion (BIC) (Schwarz, 1978). The models used in their study distinguish broadband power spectra, broadband power spectra with a kink at a specific frequency, and power spectra with enhancement in a localized frequency range. They found that the broadband ULF waves are frequently observed on the night side and they attributed the magnetic local time (MLT) dependence of the wave occurrence to wave excitation by substorm activity. They noted that the AFINO code only identifies a single wave frequency for discrete ULF waves, and a higher wave frequency tends to be selected due to the algorithm of BIC if there are two or more spectral peaks.

While the observations of monochromatic/broadband toroidal waves have been reported by both event studies (Matsui et al., 2007; Sarris, 2014; Sarris et al., 2009; Shi et al., 2020; Vellante et al., 2004) and statistical studies (Liu et al., 2009; Murphy et al., 2020; Takahashi et al., 2014; Takahashi, Hartinger et al., 2015), toroidal waves with multi-harmonic discrete frequencies have been mainly investigated in event studies (Engebretson et al., 1986, 1987; Takahashi, Denton et al., 2015; Takahashi, Hughes et al., 1984; Takahashi, Waters et al., 2015; Takahashi et al., 2020). The multi-harmonic toroidal waves (MTWs hereinafter) are considered to be standing Alfvén waves with multiple eigenmodes because the wave frequency of MTWs decreases (increases) as the L-value increases (decreases) (e.g., Engebretson et al., 1986). From the magnetic field measurements by the ATS-6 and IMP-J satellites on 1 May 1975, Takahashi, Hughes et al. (1984) demonstrated that wave power of MTWs decreased when the cone angle of the interplanetary magnetic field ( $\theta_{xB} = \cos^{-1}[B_{x, IMF}/B_{IMF}]$ ) increased up to  $\sim 80^\circ$ , where  $B_{IMF}$  is the magnitude of the interplanetary magnetic field (IMF), and the x-component of the IMF ( $B_{x, IMF}$ ) is aligned with the Sun-Earth line. In subsequent event studies (Engebretson et al., 1987; Takahashi, Waters et al., 2015; Takahashi, Denton et al., 2015; Takahashi et al., 2020), it was shown that the wave power of MTWs is enhanced when the cone angle decreased to  $< 45^\circ$ . These results indicate that the energy source of MTWs is similar to that of the dayside Pc 3–4 waves, that is, upstream waves generated by the ion beam instability (e.g., Fairfield, 1969) in the ion foreshock region because the wave power of the dayside Pc 3–4 (6.7 mHz–0.1 Hz) waves is also controlled by the cone angle (e.g., Heilig et al., 2007). In previous studies, however, the effect of the other solar wind parameters on the excitation of MTWs was not mentioned in detail. An interesting similarity between the event studies by Takahashi, Waters et al., 2015; Takahashi, Denton et al., 2015; Takahashi et al., 2020, is that MTWs were observed inside or around the plasmopause. Many event studies of MTWs focused on the relation between MTWs and the solar wind; however, examination of the effect of the local plasma environment may also provide a clue to the excitation mechanism of MTWs.

To the best of our knowledge, only two statistical studies of MTWs were conducted by Anderson et al. (1990); Anderson and Engebretson (1995) investigated spatial distributions of the occurrence rate of MTWs observed by the AMPTE/CCE satellite and showed that MTWs are frequently observed from 06 to 16 MLT. There is not a significant radial dependence of the occurrence rate of MTWs. From the spatial distribution of MTWs, they suggested that MTWs are excited by the dayside energy source and driving waves transmitted inside the magnetosphere through the cusp region. Anderson and Engebretson (1995) compared the magnetic field amplitudes between MTWs and broadband ULF waves and discussed the similarities and differences of wave amplitudes between these two types of ULF waves. Their statistical studies focused on the occurrence rate and wave power of MTWs, and hence no statistical study of solar wind dependence exists at present.

In this study, we examine the possible excitation mechanisms of MTWs by conducting a statistical analysis of solar wind dependence for the first time. One of the difficulties in the investigation of the relation between ULF waves and the solar wind is that solar wind parameters are correlated with each other, and it is difficult to determine which one controls the wave excitation. To circumvent this difficulty, we separate the solar wind conditions into four groups: high/low-speed solar wind ( $V_{SW}$  greater/less than 450 km/s) and large/small cone angle ( $\theta_{xB}$  greater/less than  $45^\circ$ ). We investigate the dependence of the occurrence rate, wave power, and frequency range of MTWs on the solar wind parameters. We further analyze the dependence on the local plasma density to reveal the effect of the plasmasphere.

The rest of this paper is organized as follows. Section 2 describes the data used in our statistics and our method for the detection of MTWs. Section 3 describes the statistical results of MTWs. Section 4 discusses the energy source of multi-harmonic toroidal waves and the plasmaspheric effect, and Section 5 concludes the study.

## 2. Data and Methodology

### 2.1. Arase Satellite Data

We used magnetic field and electron density data provided by the Arase satellite, which was launched by the Japan Aerospace Exploration Agency (JAXA) on 20 December 2016. The Arase satellite has an apogee of  $\sim 6.1 R_E$  and perigee altitude of  $\sim 400$  km. The inclination angle of the satellite orbit is approximately  $31^\circ$ . Thus, the Arase satellite sometimes covers a wide L-shell range up to  $L \sim 10$  when its apogee is located in a high magnetic latitude region (Miyoshi, Shinora, Takashima et al., 2018). The Arase satellite is spin-stabilized with a spin period of  $\sim 8$  s, and its orbital period is  $\sim 565$  min. The procession rate of its apogee is  $\sim 220^\circ/\text{year}$ . We used Arase data from 23 March 2017 to 30 September 2020. Arase has almost three times swept all MLT during this interval; therefore, the MLT coverage is wide enough to perform a statistical study. As for the L-shell value, we used McIlwain's L (McIlwain, 1961) for the IGRF-13 model (Thébault et al., 2015) provided by the data of spacecraft orbit (Miyoshi, Shinora & Jun, 2018).

The Arase satellite is equipped with a fluxgate magnetometer as hardware of the Magnetic Field Experiment (MGF) (Matsuoka, Teramoto, Nomura et al., 2018; Matsuoka, Teramoto, Imajo, et al., 2018) to measure the DC component of the ambient magnetic field. Depending on the L-shell at the satellite location, the sampling cadence of the fluxgate magnetometer is nominally switched between 64 vectors/s (for  $L > 4$ ) and 256 vectors/s (for  $L < 4$ ), and hence 64-Hz magnetic field data are provided regularly. There is another product of spin-averaged 8-s data; however, we used the 64-Hz data to cover the whole frequency range of ULF waves up to 100 mHz.

Before we performed spectral analysis of the magnetic field, we first removed the spin-tone ( $\sim 8$  s) noise from the 64-Hz data by sine curve fitting that uses a least-square method (e.g., Imajo et al., 2021). 1-s averaged data were calculated from the 64-Hz data after the noise reduction. We used the 1-s averaged data in the following spectral analysis.

Electron density data were obtained from the measurements of the upper hybrid resonance emissions by High Frequency Analyzer (HFA) of Plasma Wave Experiment onboard the Arase satellite (Kumamoto et al., 2018). The local electron density was derived from the upper hybrid resonance frequency and the magnitude of the magnetic field measured by MGF. The time resolution of the electron density data is 1 min (Kasahara et al., 2021).

### 2.2. Solar Wind Data

1-min solar wind data were obtained from the OMNIWeb database to study the relation between MTWs and the solar wind parameters. The cone angle of the IMF was calculated from the magnetic field in the GSM coordinates. To examine the relation to the solar wind dynamic pressure variations in the ULF frequency range up to 0.1 Hz, we also used 3-s plasma data provided by the 3DP instrument onboard the WIND satellite (Lin et al., 1995). The OMNI data have been time-shifted to the earth's bow shock nose by the data provider. We used the shift time of the 5-min OMNI data to robustly obtain shifted 3DP data.

### 2.3. Method of Wave Detection

In this subsection, we describe how to determine the event of MTWs. First, we defined the mean field-aligned coordinate system to separate the magnetic field fluctuation into the toroidal (azimuthal), poloidal (radial), and compressional (parallel) components. The azimuthal direction ( $\phi$ , positive eastward) is defined as the direction of  $\bar{\mathbf{B}} \times \mathbf{R}$ , where  $\bar{\mathbf{B}}$  is the 10-min averaged magnetic field vector measured by MGF, and  $\mathbf{R}$  is the position vector of the Arase satellite from the center of the Earth. The parallel direction ( $\mu$ ) is directed along  $\bar{\mathbf{B}}$ , and the radial direction ( $\nu$ , outward positive) is given by  $\mathbf{e}_\nu = \mathbf{e}_\phi \times \mathbf{e}_\mu$ , where  $\mathbf{e}$  is the unit vector of each direction. The magnetic field data were rotated into the  $\nu$ - $\phi$ - $\mu$  coordinate system.

In previous studies, event detection of ULF waves has been conducted visually or automatically. Takahashi et al. (2014) detected fundamental toroidal ULF waves by computing fast Fourier transform (FFT) spectra of the plasma bulk velocity measured by the Geotail satellite and selecting spectral peaks with narrow full width at half maximum. Anderson et al. (1990) performed a statistical study of the occurrence of MTWs by a visual scan of the magnetic field spectra obtained from AMPTE/CCE satellite measurements, while Nosé et al. (2015) detected

spectral peaks of MTWs by comparing power spectral density (PSD) at a local peak to that around the peak in their event study.

In this study, we calculated FFT power spectra of the magnetic field with a window width of 2,048 s and a window shift of 256 s, and hence, the frequency resolution ( $\Delta f$ ) is  $\cong 0.49$  mHz. From the calculated spectra, we automatically detected multi-harmonic toroidal waves to conduct a statistical analysis without bias of visual inspection. A couple of criteria were used to select spectral peaks from  $B_\phi$  power spectra as toroidal ULF wave events for each time step of the power spectra: (a) The PSD at the selected peak in the  $B_\phi$  spectra ( $\text{PSD}_\phi(f_{\text{peak}})$ ) is greater than  $3.0 \text{ nT}^2/\text{Hz}$ , which enables detection of weak emissions of ULF waves at high harmonics. (b)  $\text{PSD}_\phi(f_{\text{peak}})/\text{PSD}_v(f_{\text{peak}}) > 1$  for toroidal mode waves, where  $\text{PSD}_v$  is the power spectral density at the selected peak in the  $B_v$  spectra. (c) The frequency of the selected peak is between 1.6 and 100 mHz. (d) The PSD around the selected peak satisfies  $\text{PSD}_\phi(f_{\text{peak}})/\text{PSD}_\phi(f_{\text{peak}} \pm C\Delta f) > 1.0$ ,  $\text{PSD}_\phi(f_{\text{peak}})/\text{PSD}_\phi(f_{\text{peak}} \pm 2C\Delta f) > 1.3$ ,  $\text{PSD}_\phi(f_{\text{peak}})/\text{PSD}_\phi(f_{\text{peak}} \pm 3C\Delta f) > 1.5$ ,  $\text{PSD}_\phi(f_{\text{peak}})/\text{PSD}_\phi(f_{\text{peak}} \pm 4C\Delta f) > 1.3$ ,  $\text{PSD}_\phi(f_{\text{peak}})/\text{PSD}_\phi(f_{\text{peak}} \pm 5C\Delta f) > 1.0$ , where  $f_{\text{peak}}$  is the frequency of the selected peak, and  $C$  is a coefficient that depends on a modeled eigenfrequency of toroidal ULF waves. The procedure for the determination of  $C$  is described below.

Following the manner of Nosé et al. (2015), the eigenfrequency of toroidal oscillations of a field line was calculated from the magnetic field model of Tsyganenko (1989) and the MHD wave equation derived by Singer et al. (1981). In this calculation, we assumed the plasma density distributions as  $n(R) = n_{\text{eq}}(R_{\text{eq}}/R)^\alpha$  and  $\alpha = 0.5$ , where  $n$  is the plasma density at a spacecraft position,  $n_{\text{eq}}$  is the equatorial plasma density, and  $R_{\text{eq}}$  is the radial distance to the field line at the equator. Because of the quasi-neutrality of plasma, we regarded the electron density measured by HFA as the plasma density at the position of Arase. Proton plasma is also assumed to obtain plasma mass density.

The coefficient  $C$  in the criterion (d) was determined from the calculated eigenfrequencies of fundamental and the second harmonic toroidal modes ( $f_{T1}^{\text{model}}$  and  $f_{T2}^{\text{model}}$ ). To exclude local spectral peaks that are not related with the field line resonance, we chose  $C$  as  $5C\Delta f = 0.3(f_{T2}^{\text{model}} - f_{T1}^{\text{model}})$ ; that is, 30% of the interval of modeled eigenfrequencies was used as the size of the side robe around the spectral peak. We assumed proton plasma ( $M_{\text{ave}} = 1$  a.m.u., where  $M_{\text{ave}}$  is the averaged plasma mass) in the model calculation; however, the observed frequency interval of ULF wave emissions is sometimes narrower than the model because heavy ions lower the eigenmode frequency. Therefore, we used 30% of the interval in the model calculation, which corresponds to the frequency interval for  $M_{\text{ave}} \sim 11$ , to ensure that MTWs can be detected in heavy-ion-rich plasma, which often appears during the main and recovery phases of geomagnetic storms (e.g., Horwitz et al., 1984; Nosé et al., 2015; Takahashi et al., 2008). If there were no density data and the eigenfrequencies could not be calculated, we gave  $C = 1$ .

After selecting the spectral peaks by applying the above criteria, we excluded selected peaks that are created by instances of high artificial noise. The artificial noise has constant frequencies at  $\sim 3$ ,  $\sim 27$ , and  $\sim 33$  mHz, corresponding to Pc 3 and Pc 5 ranges. They often appear in the magnetic field perpendicular to the spin axis for dayside measurements of Arase (not shown), but the cause of the noise is unclear at present. Therefore, we just excluded the selected peaks at  $\sim 3$ ,  $\sim 27$ , and  $\sim 33$  mHz from our statistics regardless of whether the selected peak is a real peak of ULF waves or not. This process may cause exclusion of fundamental toroidal mode waves in Pc 5 range at higher L-shell.

In addition, we focused on the magnetic field measurements at  $R$  greater than  $3.5 R_E$  and MLT from 06 to 18 hr because event studies and a statistical study have revealed that MTWs are mainly observed on the dayside (Anderson et al., 1990; Engebretson et al., 1986; Takahashi, Hughes et al., 1984). In the night sector, magnetic field disturbances related to substorms or geomagnetic storms tend to contaminate the statistical result of ULF wave detection (e.g., Takahashi et al., 1996). That is the other reason we excluded the nightside events of MTWs from our statistical study. However, we should note that there is a report of an unusual event of MTWs observed around midnight (Takahashi et al., 2020).

Finally, we defined multi-harmonic wave events as the time steps when the number of the selected peaks is greater than two. We also categorized the time steps when a single frequency is selected as monochromatic wave events. To separate the energy sources of MTWs, we investigated the wave occurrence frequency and wave power at each L-shell and MLT bin with a bin size of  $1 R_E$  and 1 hr under four conditions of  $V_{\text{SW}}$  and  $\theta_{xB}$ .

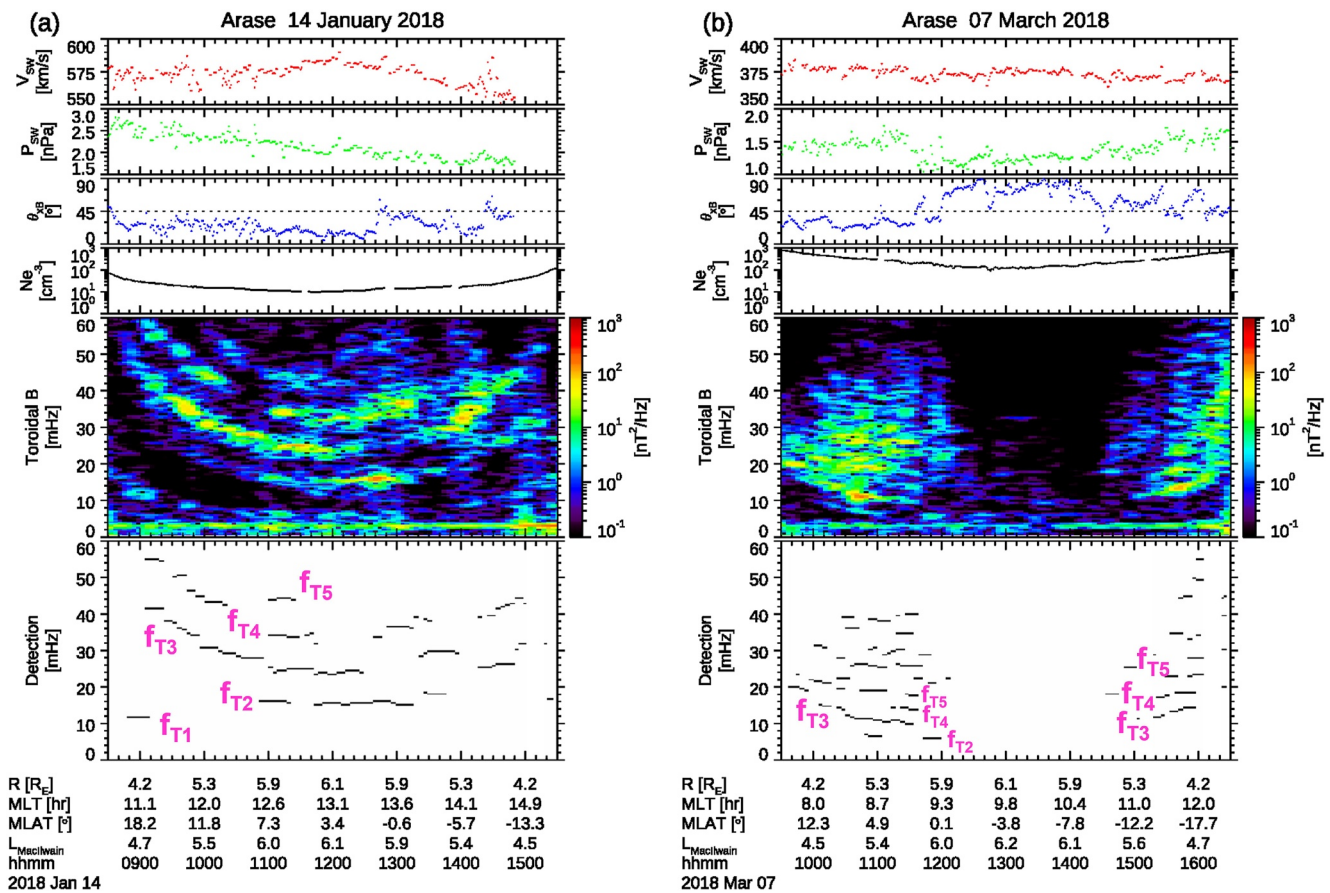


**Figure 1.** Examples of multi-harmonic toroidal ultra-low frequency (ULF) waves. (a) The three panels at the top show the flow speed ( $V_{sw}$ ), dynamic pressure ( $P_{sw}$ ), and clock angle ( $\theta_{sB}$ ) of the solar wind from the OMNI data on 14 January 2018. The fourth panel shows the electron density at the Arase satellite. The fifth panel presents the dynamic power spectral density of  $B_\phi$  measured by MGF onboard the Arase satellite. The bottom panel shows the frequency of the spectral peaks selected by our procedure of ULF wave detection. “ $f_{T1}$ ,” “ $f_{T2}$ ,” ..., “ $f_{T5}$ ” represent the frequencies of the fundamental to the fifth harmonic mode. (b) Same format as Figure 1a except that the date is 07 March 2018.

### 3. Results

#### 3.1. Examples of Multi-Harmonic Toroidal Wave Events

Here, we show two examples of MTWs detected by our method described in the previous section. Figure 1a shows MTWs and selected peaks of the wave emissions during high-speed solar wind and small cone angle on 14 January 2018. Because a co-rotating interaction region (CIR) reached around the Earth and the solar wind speed started to increase at 19 UT on 13 January 2018, the solar wind speed exceeds 550 km/s as shown in the first panel from the top. The dynamic pressure of the solar wind is moderate ( $\sim 2$  nPa) and gradually decreases (the second panel). The cone angle of the IMF is almost less than  $45^\circ$  and often becomes less than  $30^\circ$  (the third panel). The Arase satellite was located outside the plasmasphere in this event (the fourth panel). Arase moved from 11 MLT to 15 MLT and observed harmonic toroidal waves up to the sixth harmonic as shown in the  $B_\phi$  spectrum (the fifth panel). Even mode waves are prominent around the magnetic equator ( $|MLAT| < 10^\circ$ ) between 11:00 UT and 13:20 UT. The third harmonic waves are intensified away from the equator. In the fifth panel, artificial noise with a constant frequency can be seen at  $\sim 3$  mHz. Selected peaks of the  $B_\phi$  spectrum are depicted in the sixth panel.

Figure 1b shows the case of low-speed solar wind on 7 March 2018. The flow speed is constant at  $\sim 375$  km/s (the first panel), while the cone angle dramatically changes from less than  $45^\circ$  up to  $\sim 90^\circ$  during 12:00–14:30 UT (the second panel). As for this event, the Arase satellite was inside the plasmasphere in the pre-noon sector (the fourth panel). MTWs appear in the  $B_\phi$  spectrum before 12 UT and after 15 UT (the fifth panel). Discrete spectral peaks from the second harmonic to greater than the fifth harmonic are embedded in the broadband spectra. The period

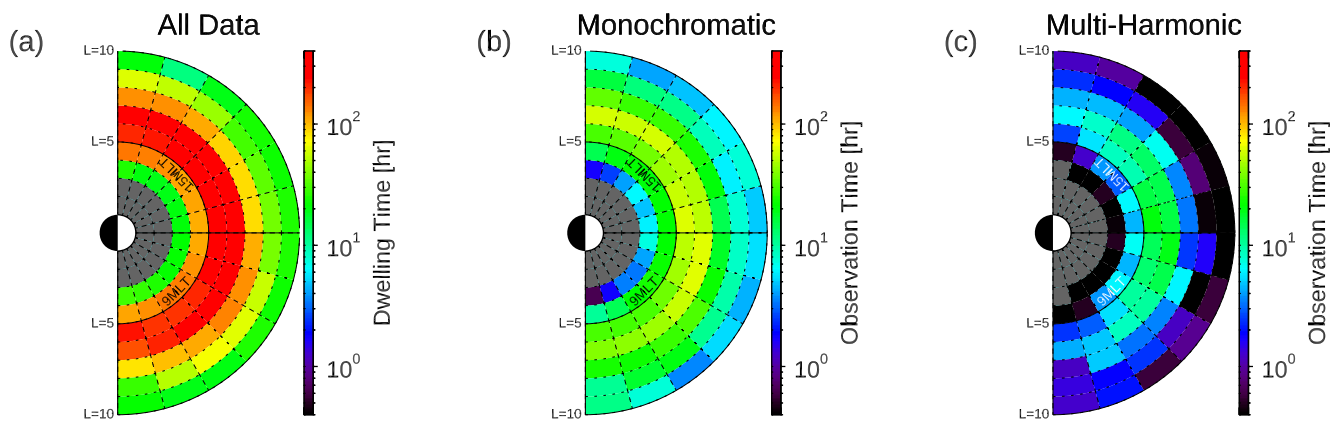


**Figure 2.** (a) L-MLT distributions of the dwelling time of the Arase satellite between 23 March 2017 and 31 September 2020. (b) L-MLT distributions of the observation time of monochromatic toroidal waves. (c) Same as Figure 2b except for multi-harmonic toroidal waves. Gray indicates the region where there is no event or the outside of the coverage our statistics ( $R < 3.5 R_E$ ).

in which MTWs disappear seems to correspond to that of a large cone angle ( $\theta_{xB} > 60^\circ$ ). This feature of MTWs is the same as that reported by Takahashi, Hughes et al. (1984).

Based on these examples, several solar wind parameters probably influence the occurrence of MTWs, and the plasma density (electron density) changes the broadness of the frequency spectra of the waves. In the next subsections, we examined the statistical properties of MTWs to understand their dependence on the solar wind and local plasma density.

### 3.2. L-MLT Distributions of the Occurrence Rate and Wave Power

Figure 2 presents the dwelling time of the Arase satellite and observation time of the monochromatic events and MTWs on the L-shell and MLT plane for the data period from 23 March 2017 to 30 September 2020. The dayside is shown to the right of the L-MLT plane. The Arase satellite covers a wide L-shell range up to  $\sim 10$ , and the most frequent L-shell value is 6–7 (Figure 2a). Figures 2b and 2c show the total observation time of monochromatic waves and MTWs for all frequency range. In Figure 2 and the following figures, we do not distinguish the frequency band (Pc 3–5) of the detected waves because the frequencies of MTWs often extend over more than two frequency bands as seen in Figure 1. The observation time of the MTWs is several times shorter than that of the monochromatic waves. Since the observation time of MTWs at higher L-shell bins is too short to interpret statistical results of the waves at these bins, we mask the bins where the observation time of the monochromatic waves or MTWs is less than 20 min in the following results.

Figure 3 shows the L-MLT distributions of the occurrence rate of the monochromatic toroidal waves (four panels on the left side) and the multi-harmonic toroidal waves (four panels on the right side) under four conditions of the flow speed and the cone angle of the solar wind. As for the monochromatic waves, the occurrence rate is enhanced on the flank sides at  $L = 7–10$  as shown in Figures 3b and 3d, implying that the energy source of these waves is the Kelvin Helmholtz (KH) instability. From Figures 3a and 3c, the occurrence rate of the monochromatic waves is globally enhanced when the solar wind velocity is high ( $V_{sw} > 450$  km/s) and the cone angle is small ( $\theta_{xB} < 45^\circ$ ). In the case of the high-speed solar wind, the occurrence rate of the monochromatic waves around noon increases as the cone angle becomes small (Figures 3a and 3c). Comparing with the monochromatic waves, the occurrence rate of MTWs shows a clear dependence of the MLT distributions on the solar wind conditions. For the low-speed solar wind ( $V_{sw} < 450$  km/s) and small cone angle, the occurrence rate of MTWs is low and does not show large variations in MLT (Figure 3f). When the cone angle becomes small, the occurrence rate around noon increases at all L-shell ranges (Figure 3h). This tendency is also seen in the case of the high-speed solar wind (Figures 3e and 3g). Therefore, the cone angle controls the occurrence of MTWs around noon. Monochromatic waves do not show such a clear dependence on the cone angle in the case of low-speed solar wind. When the solar wind speed is high and the cone angle is large ( $\theta_{xB} > 45^\circ$ ), the occurrence rate is enhanced on the flank sides (Figure 3e), which seems to be a characteristic of the waves driven by the KH instability.

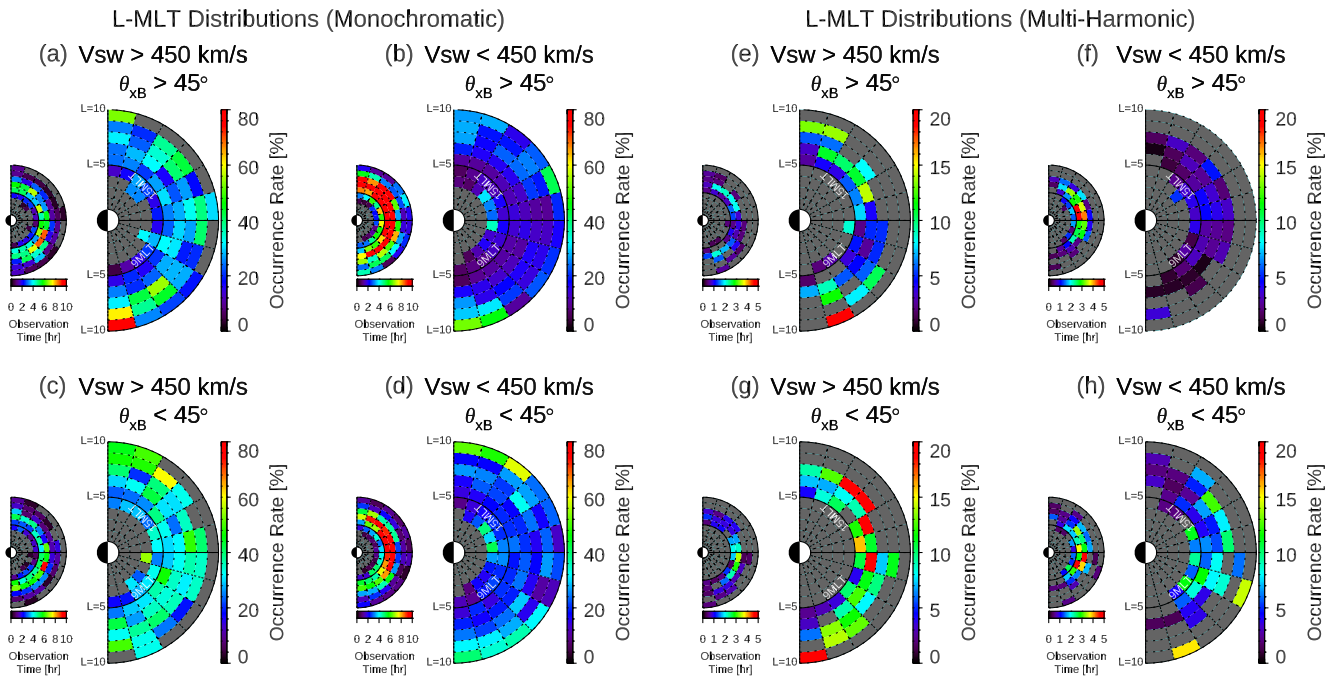


**Figure 3.** (a)–(d) L-MLT distributions of the occurrence rate of monochromatic toroidal waves for four types of solar wind conditions: (a)  $V_{sw} > 450$  km/s and  $\theta_{xB} > 45^\circ$ , (b)  $V_{sw} < 450$  km/s and  $\theta_{xB} > 45^\circ$ , (c)  $V_{sw} > 450$  km/s and  $\theta_{xB} < 45^\circ$ , and (d)  $V_{sw} < 450$  km/s and  $\theta_{xB} < 45^\circ$ . (e)–(h) Same format as Figures 3a–3d except for multi-harmonic waves. Gray indicates the region where the observation time is less than 20 min or outside of the coverage of our statistics ( $R < 3.5 R_E$ ). The small semicircles present observation time.

Figure 4 shows the L-MLT distributions of the power spectral density at the detected peak in the  $B_\phi$  spectra. In the panels of the multi-harmonic waves, the wave power averaged over all multiple peaks is presented. For both the monochromatic waves and multi-harmonic waves, the wave power on the flank sides is larger than that in the noon sector at  $L > 6$  (Figures 4a–4e, and 4g). The wave power increases as the flow speed of the solar wind increases for all cases. This result suggests that the monochromatic waves and MTWs on the flank sides are driven by the KH instability. The wave power of the monochromatic waves shows a dawn-dusk asymmetry, which is a characteristic of toroidal Pc 5 waves observed in space and on the ground (e.g., Cao et al., 1994; Gupta, 1975; Nosé et al., 1995; Olsen & Rostoker, 1978). While the occurrence rate of MTWs in the noon sector increases when the cone angle is small, the wave power of MTWs does not change (Figures 4c and 4g, or Figures 4f and 4h). Thus, the cone angle seems to control only the occurrence of MTWs. We further analyzed the clock angle dependence of MTWs, but we did not find a significant change in the MTW activities.

The L-MLT distributions of maximum and total wave power of the detected peaks were also examined for MTW events. The distributions were not changed significantly, suggesting the definition of wave power is not influential in this study. It should be noted that Arase's observations of the magnetic latitude at higher L-shell bins ( $L > \sim 7$ ) are limited in off-equator ( $IMLAT > 10^\circ$ ) regions. At the higher L-shells, MTWs with large amplitudes probably include fundamental mode waves excited by the Kelvin-Helmholtz instability (e.g., Takahashi, Hartinger et al., 2015), whose magnetic field amplitudes become small at the magnetic equator. Therefore, the averaged wave power shown in Figure 4 of the manuscript may be larger than the averaged wave power that is obtained from data including the equatorial observations at  $L > \sim 7$ .

### 3.3. Dependence on the Solar Wind Dynamic Pressure and Local Electron Density

We further investigated the influence of the solar wind dynamic pressure. Figure 5 presents the occurrence rate of MTWs as a function of the power spectral density of the proton dynamic pressure measured by the WIND satellite ( $P_{WIND}$ ). The power spectral density of  $P_{WIND}$  ( $PSD_{P_{WIND}}$ ) was averaged over the ULF wave frequency range (1.67–100 mHz). The averaged power was separated into logarithmic bins with a bin size of 0.5. The occurrence rate was calculated for multi-harmonic events in all L-shell and MLT ranges. To exclude the effect of the solar



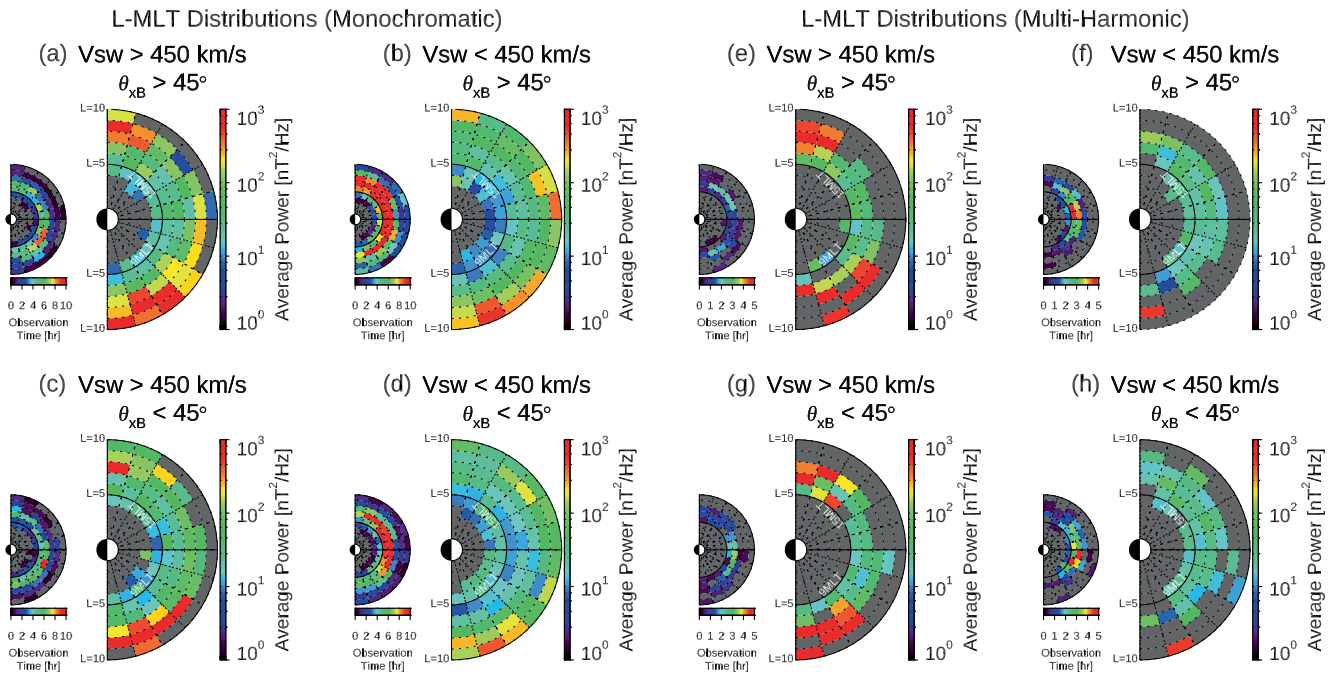


**Figure 4.** (a)–(d) L-MLT distributions of the power spectral density of  $B_\phi$  at the peak frequency of monochromatic toroidal waves for four types of solar wind conditions: (a)  $V_{sw} > 450$  km/s and  $\theta_{xB} > 45^\circ$ , (b)  $V_{sw} < 450$  km/s and  $\theta_{xB} > 45^\circ$ , (c)  $V_{sw} > 450$  km/s and  $\theta_{xB} < 45^\circ$ , and (d)  $V_{sw} < 450$  km/s and  $\theta_{xB} < 45^\circ$ . (e)–(h) The same format as Figures 4a–4d except for the power spectral density of multi-harmonic waves averaged over selected peaks.

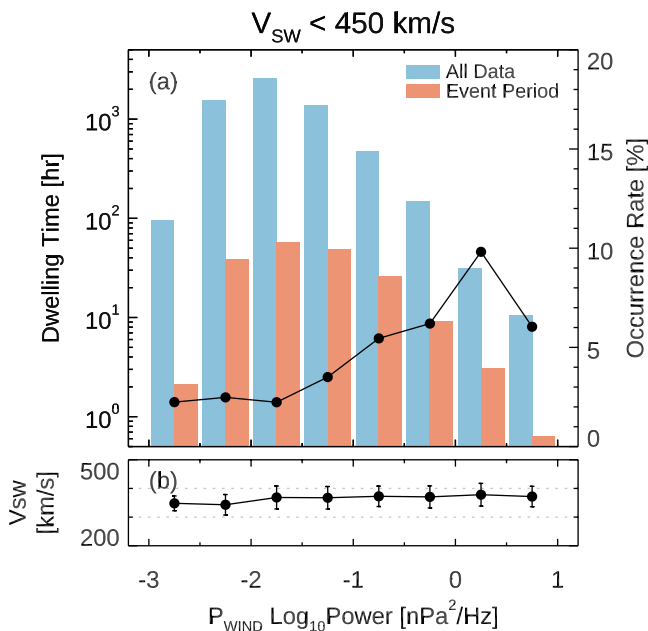


**Figure 5.** (a) Observation time and occurrence rate of the multi-harmonic toroidal waves as a function of the power spectral density of the solar wind dynamic pressure averaged over 1.67–100 mHz. The blue bar represents the dwelling time of the Arase satellite. The red bar represents the observation time of the multi-harmonic waves. The solid line is the occurrence rate of the multi-harmonic toroidal waves. (b) Averaged solar wind speed for each PSD bin of the solar wind dynamic pressure. Only the data of  $V_{sw} < 450$  km/s were used.

wind speed, only the interval of  $V_{sw} < 450$  km/s was analyzed. Averaged solar wind speed for each  $P_{WIND}$  fluctuation level is shown in Figure 5b. The solar wind speed is between 350 and 400 km/s, and hence we consider that the solar wind speed is low and constant enough to exclude the effect of the high-speed solar wind from the analysis. The occurrence rate increases from 2% to 10% as  $PSD_{P_{WIND}}$  becomes large (Figure 5a). The observation time of MTWs is less than 1 hr at the bin of the largest  $P_{WIND}$  fluctuation ( $0.5 < \log_{10} PSD_{P_{WIND}} [nPa^2/Hz] < 1.0$ ), and hence the decrease of the occurrence rate at this bin may be unreliable. We also checked the influence of the solar wind dynamic pressure on L-MLT distributions of the occurrence rate to MTWs, but there was no L-shell and MLT dependence of the occurrence rate.

The relation between MTWs and the electron density at the Arase satellite was also examined. Figure 6a shows the occurrence rate of MTWs as a function of the electron density. MTWs are frequently observed for  $N_{e,Arase} \lesssim 1$   $cm^{-3}$  and  $N_{e,Arase} \gtrsim 100$   $cm^{-3}$ . Wave power of  $B_\phi$  and  $B_\mu$  averaged over selected peaks is shown in Figure 6b. The electron density dependence of the wave power of  $B_\phi$  is different from that of the occurrence rate of MTWs. The wave power of  $B_\phi$  rapidly decreases as the electron density increases even though the occurrence rate increases again in the high-density region. There is a positive correlation between  $B_\phi$  and  $B_\mu$  power at  $N_{e,Arase} < 10$   $cm^{-3}$ . The positive correlation in the low-density region may be attributed to the leakage of the large toroidal power or the uncertainty of the background magnetic field direction. In the low-density ( $N_{e,Arase} < 10$   $cm^{-3}$ ) periods of MTW observations, the solar wind speed is greater than  $\sim 450$  km/s (Figure 6c). Therefore, the high occurrence rate and large wave power when the electron density is low are associated with the KH instability; that is, in the low-density period, the Arase satellite may be located at higher L-shell (low density regions)

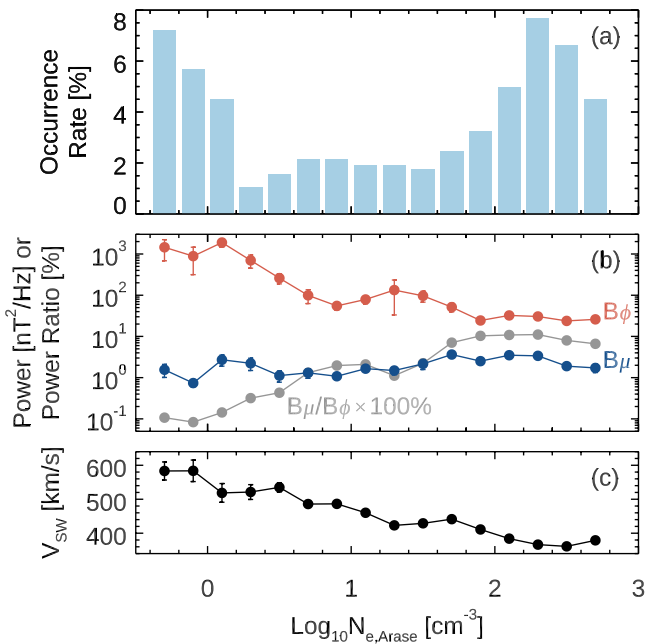


**Figure 6.** (a) Occurrence rate of the multi-harmonic toroidal waves as a function of the electron density at the position of the Arase satellite. (b) Power spectral density of the azimuthal (red line) and compressional (blue line) magnetic fields averaged over the spectral peaks of the multi-harmonic toroidal waves. The gray line indicates the ratio of the compressional power to the toroidal power. (c) Averaged solar wind velocity. The error bar represents the standard error.

and observes ULF waves driven by the KH instability around the flankside magnetopause. It is also possible that the plasmasphere shrinks and the electron density decreases when ULF waves driven by the KH instability are observed under the condition of high-speed solar wind (e.g., He et al., 2017; Larsen et al., 2007). At  $N_{e,Arase} > 10$  cm<sup>-3</sup>, the wave power of  $B_{\mu}$  gradually increased from  $\sim 1$  nT<sup>2</sup>/Hz and has a broad peak of  $\sim 4$  nT<sup>2</sup>/Hz around 100 cm<sup>-3</sup>, while the  $B_{\phi}$  power may have a local maximum at  $\sim 20$  cm<sup>-3</sup> ( $\text{log}_{10} N_{e,Arase} \sim 1.3$ ). Section 4.2 provides detailed discussion of the enhancement of the occurrence rate in the high density period.

### 3.4. Property of Wave Frequency

In this subsection, we examined the frequency property of MTWs. Since MTWs have a wide frequency range and often appear in multiple frequency bands, we analyzed the minimum, median, and maximum frequencies of the frequency band of MTWs. Figure 7 shows the observation time of the minimum frequency ( $f_{min}$ ) of detected peaks. In Figure 7,  $f_{min}$  is normalized with the model frequency of fundamental toroidal mode, which was calculated in the manner described in Section 2.3. The ticks in the horizontal axis of Figure 7 depict the most frequent values of the ratio between the model frequencies of the fundamental mode and the second to sixth harmonic modes to determine the harmonic structure of the wave observed at  $f_{min}$ . The most frequent ratios for each harmonic mode are as follows:  $f_{T2}^{model}/f_{T1}^{model} = 2.5$ ,  $f_{T3}^{model}/f_{T1}^{model} = 4.1$ ,  $f_{T4}^{model}/f_{T1}^{model} = 5.5$ ,  $f_{T5}^{model}/f_{T1}^{model} = 7.1$ , and  $f_{T6}^{model}/f_{T1}^{model} = 8.7$ . These values are almost identical to the result of Takahashi and Denton (2021) for  $\alpha = 0.5$  within the differences of  $\pm \sim 0.1$ . In Figure 7a, all data periods were used for the histogram of  $f_{min}$ . The first three peaks of the observation time at  $f_{min}/f_{T1}^{model} = 1.1, 2.7$ , and 4.3 correspond to the fundamental to the third harmonic waves. The peak of observation time of the

fourth harmonic wave may be seen slightly beyond  $f_{min}/f_{T1}^{model} = 5.5$ . We separated the frequency ratio into three groups of the magnetic latitude (MLAT). The fundamental mode waves are most frequently observed at  $f_{min}$  in the off-equator region ( $|\text{MLAT}| > 20^\circ$ ) (Figure 7b). In the intermediate region ( $10^\circ < |\text{MLAT}| < 20^\circ$ ), the third harmonic waves seem to be dominant (Figure 7c). In the equator region ( $|\text{MLAT}| < 10^\circ$ ), the second harmonic mode is prominent (Figure 7d). This latitudinal dependence is consistent with the node structure of standing Alfvén waves (e.g., Takahashi & Denton, 2021).

We also compared the median value of the multi-harmonic frequencies ( $f_{med}$ ) with the theoretical frequency of the upstream waves ( $f_{UW}$ ) in the time interval of  $\theta_{xB} < 45^\circ$ . The upstream wave frequency was calculated from the equation derived by Takahashi, Teresawa et al. (1984):

$$f_{UW}[\text{mHz}] = 7.6 \times B_{IMF}[\text{nT}] \cos^2 \theta_{xB} \quad (1)$$

Figures 8a and 8b represent the observation time of MTWs as a function of  $f_{med}$  and  $f_{UW}$  in the noon sector ( $09 < \text{MLT} < 15$  hr) and flank sector ( $06 < \text{MLT} < 09$  hr and  $15 < \text{MLT} < 18$  hr), respectively. In the noon sector,  $f_{med}$  is roughly identical to  $f_{UW}$  in the frequency range from  $\sim 10$  to  $\sim 45$  mHz. On the flank sides, however, the linearity between  $f_{med}$  and  $f_{UW}$  is not as clear as the noon sector at higher frequencies. The correlation coefficients (C.C.) between  $f_{med}$  and  $f_{UW}$  are 0.49 and 0.22 in the noon sector and flank sides, respectively. Compared with the noon sector, the distributions of  $f_{med}$  on the flank sides are not symmetrical to the white dashed line in Figure 8b, which presents the line of  $f_{med} = f_{UW}$ . The median frequency of  $f_{med} < f_{UW}$  seems to be observed more frequently than  $f_{med} > f_{UW}$  in this region.

Finally, we present the variations of the maximum frequency of MTWs ( $f_{max}$ ). To represent the broadness of the power spectrum of  $P_{WIND}$ ,  $\text{PSD}_{P_{WIND}}$  at the ULF wave frequency range (1.67 mHz–0.1 Hz) was approximated into a straight line in log-log space by the least squares method. The frequency at which the approximated line decreases to 0.01 nPa<sup>2</sup>/Hz was defined as  $f_{fit}$ . Figure 9 shows a couple of examples of this procedure. In this analysis, we analyzed the data when the electron density observed by Arase was less than 50 cm<sup>-3</sup> to reduce

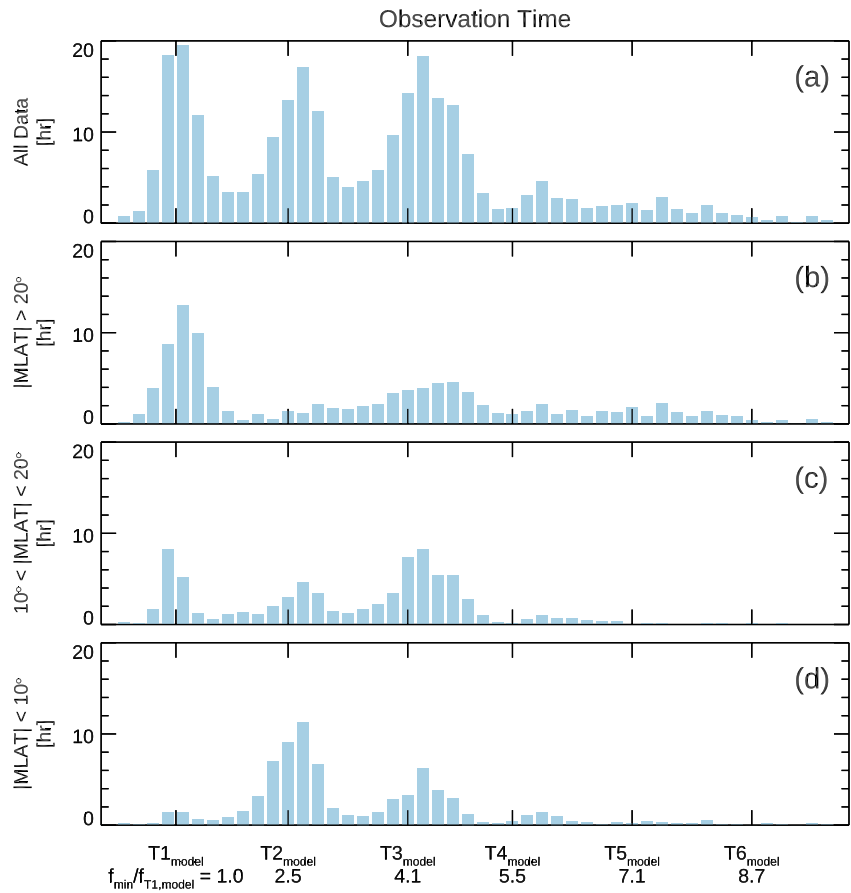


**Figure 7.** Observation time of the multi-harmonic toroidal waves as functions of the minimum frequency of the observed waves normalized with the model frequency of the fundamental toroidal standing Alfvén waves ( $f_{T1_{\text{model}}}$ ) for (a) all data, (b)  $|\text{MLATI}| > 20^\circ$ , (c)  $10^\circ < |\text{MLATI}| < 20^\circ$ , and (d)  $|\text{MLATI}| < 10^\circ$ . MLAT means the magnetic latitude of the spacecraft. The labels  $T1_{\text{model}}, T2_{\text{model}}, \dots, T6_{\text{model}}$  indicate the most frequent values of the ratio of the harmonic eigenfrequencies to the fundamental frequency.

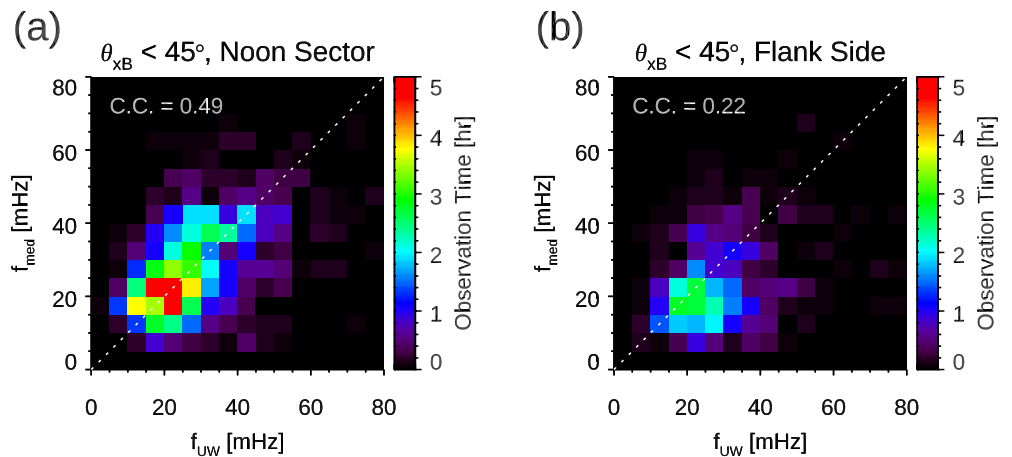


**Figure 8.** Observation time of the multi-harmonic toroidal waves as functions of the predicted upstream wave frequency and median frequency of the observed wave (a) in the noon sector ( $09 < \text{MLT} < 15$  hr) and (b) flank sides ( $06 < \text{MLT} < 09$  hr,  $15 < \text{MLT} < 18$  hr). Only the data of  $\theta_{xB} < 45^\circ$  were used.

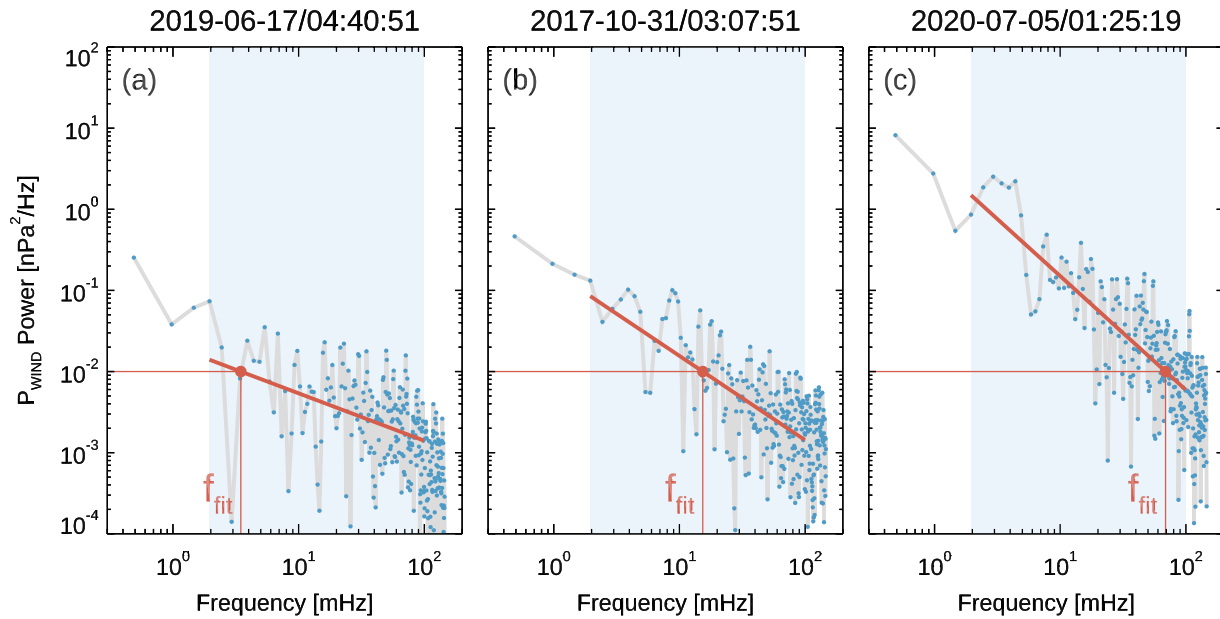


**Figure 9.** Examples of the procedure to defined  $f_{\text{fit}}$ . The blue dots represent power spectral density of the dynamic pressure observed at the WIND satellite. The red line represents the approximated line in the ultra-low frequency wave range (the frequency range shaded with blue).

the variation of  $f_{\text{max}}$  due to the electron density. Figure 10a shows the observation time of MTWs and averaged  $f_{\text{max}}$  for each  $f_{\text{fit}}$  bin. The averaged  $f_{\text{max}}$  increases from  $\sim 25$  to  $\sim 42$  mHz as  $f_{\text{fit}}$  increases from 0 to 10 mHz to 70–80 mHz. The maximum frequency of MTWs is positively correlated with the broadness of the  $P_{\text{WIND}}$  spectrum, but the variation of  $f_{\text{max}}$  ( $\sim 20$  mHz) is much smaller than that of  $f_{\text{fit}}$  ( $\sim 80$  mHz). If the broadness of the  $P_{\text{WIND}}$  spectrum controls the broadness of MTWs, the variation of  $f_{\text{fit}}$  and  $f_{\text{max}}$  should be identical. Therefore, we consider that the broadness of the  $P_{\text{WIND}}$  spectrum does not necessarily correspond to  $f_{\text{max}}$  or the broadness of the spectra of MTWs.

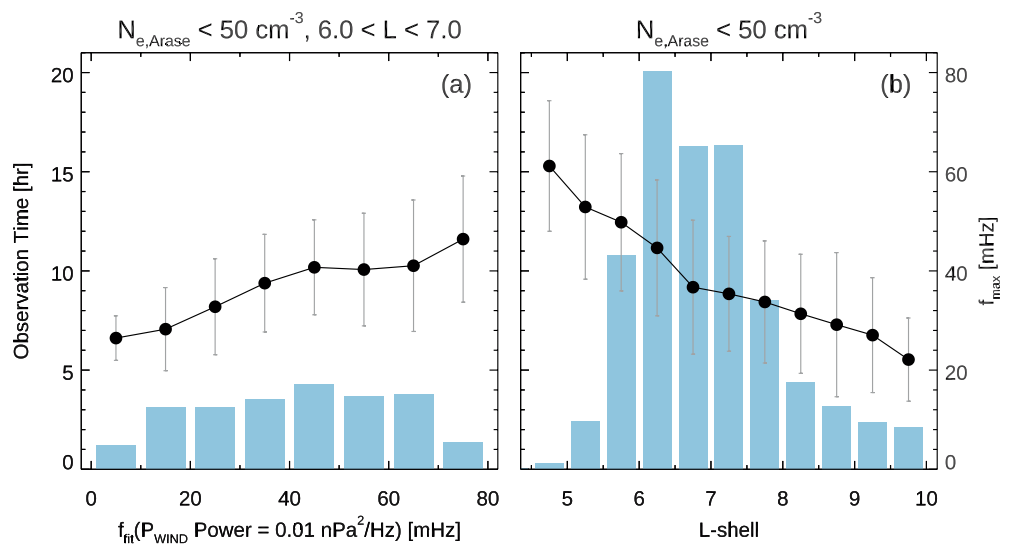


**Figure 10.** Observation time (blue bar) and the maximum frequency (solid line) of the multi-harmonic waves as functions of (a) the frequency at which the fitting line of the power spectrum of solar wind dynamic pressure fluctuations crosses 0.01 nPa<sup>2</sup>/Hz and (b) L-shell values. The error bar represents the standard deviations. Only the data of  $N_{e,\text{Arase}} < 50 \text{ cm}^{-3}$  were used.

The variation of  $f_{\max}$  is more prominent if we sorted it with L-shell values of the Arase satellite. Figure 10b shows the observation time and the averaged  $f_{\max}$  for each L-shell bin. The averaged  $f_{\max}$  decreases with the increase of the L-shell value. This tendency is similar to the eigenfrequency of standing Alfvén waves. The variation of the averaged  $f_{\max}$  is  $\sim 40$  mHz, which is about twice the variation for the fluctuation of the solar wind dynamic pressure. The interpretation of the variation of  $f_{\max}$  is discussed in Section 4.3.

## 4. Discussion

ULF waves have several kinds of energy sources. Toroidal mode waves in the dayside magnetosphere are considered to be excited by external energy sources such as the KH instability at the magnetopause (Mathie & Mann, 2001; Singer et al., 1977) and periodic/impulsive variations of the solar wind dynamic pressure (Kepko et al., 2002; Takahashi & Ukhorskiy, 2007; Zhang et al., 2010). The upstream waves penetrating inside the magnetosphere also cause azimuthal magnetic field oscillations as well as compressional oscillations (e.g., Odera et al., 1991; Takahashi et al., 2016). In the previous studies, only the cone angle dependence of MTWs was investigated and the upstream waves were considered to be the energy source of MTWs. Our statistical results of L-MLT distributions suggest that there are a couple of energy sources of MTWs. All of the KH instability, upstream waves, and fluctuations of solar wind dynamic pressure are probably the energy sources of MTWs. The dominant energy source is different between the noon sector and the flank sides. On the flank sides at  $L > \sim 6$ , the occurrence rate and wave power of MTWs exhibit the characteristics of toroidal waves driven by the KH instability (Figures 3 and 4). Since, the occurrence rate of MTWs did not show MLT dependence when the fluctuations of the solar wind dynamic pressure are high, we consider that the dynamic pressure fluctuations can excite MTWs globally on the dayside. We discuss the excitation mechanisms of MTWs in the following subsections.

### 4.1. KH Instability

As demonstrated in the MLT dependence of the occurrence rate and the wave power, the dominant excitation mechanism of the multi-harmonic waves is the KH instability on the flank sides (Figures 3 and 4). The correlation between the median wave frequency of MTWs and the predicted upstream waves frequency is weak (C.C. = 0.22, Figure 8b) on the flank sides, suggesting that the relation to the upstream waves in that region is weaker than that in the noon sector (C.C. = 0.49, Figure 8a). Because the median frequency of MTWs is relatively low ( $f_{\text{med}} < f_{\text{UW}}$ ) in the flank side observations, fundamental mode oscillations, which frequently appear in the observations of toroidal waves driven by the KH instability (e.g., Takahashi et al., 2014, Takahashi, Hartinger et al., 2015), may lower the median frequency of MTWs. MTWs which seem to be driven by the KH instability are dominantly seen outside the plasmasphere (Figures 6b and 6c). This is because the plasmasphere shrinks when the solar wind speed is high and the magnetosphere is disturbed.

Although the KH instability is probably the dominant energy source of MTWs on the flank sides, we should note the possibility that the upstream waves are observed simultaneously with the waves driven by the KH instability and consist of multiple spectral peaks because the median frequency of MTWs is almost identical around 20 mHz. The KH instability may be stimulated by the upstream disturbances of the ion foreshock which penetrate around the magnetopause (Nosé et al., 1995). Assuming that only the KH instability is the energy source of MTWs, an explanation of wave excitation at multiple frequencies is required because the KH surface wave may be originally a monochromatic source. There are two possible mechanisms: one is the magnetopause fluctuation that causes the broadening of the wave spectra (Lee & Lysak, 1991). The other possibility is that the KH surface wave originally oscillates at multiple frequencies as numerically simulated by Claudepierre et al. (2008), but it is the case of the high-speed solar wind ( $V_{\text{SW}} = 800$  km/s) in their simulation. We consider boundary oscillation as the more plausible mechanism.

### 4.2. Upstream Waves

In the noon sector ( $09 < \text{MLT} < 15$  hr), the cone angle dependence of the occurrence rate of MTWs (Figure 3) and the correspondence between  $f_{\text{med}}$  and  $f_{\text{UW}}$  in the wide frequency range (Figure 8a) is evidence of the relation between MTWs and the upstream waves. These results support the scenario that broadband fast mode waves generated in the ion foreshock region propagate into the magnetosphere through the subsolar magnetopause, and then the propagating waves are coupled with toroidal standing Alfvén mode at multiple eigenfrequencies

within the broadband spectrum through field line resonance (Takahashi, Hughes et al., 1984; Takahashi, Denton et al., 2015). If it is the case, MTWs may be frequently observed in a high local plasma (mass) density region because the interval of eigenmode frequencies of standing Alfvén waves become small and multiple eigenmodes within the finite frequency band of the upstream waves would be excited. This is possibly one of the reasons for the high occurrence rate of MTWs at  $N_{e,Arase} \gtrsim 100 \text{ cm}^{-3}$  (Figure 6). Another possible reason for the high occurrence rate in the high-density region is that the fast mode waves are trapped in the dayside plasmasphere as suggested by Takahashi et al. (2010), and the mode coupling between the trapped fast mode and toroidal mode through field line resonance can occur as reported by Keiling et al. (2001). In our study, the power spectral density of the compressional magnetic field component shows the broad local maximum around  $N_{e,Arase} \sim 100 \text{ cm}^{-3}$  (Figure 6b). The ratio of the wave power between the compressional and toroidal magnetic fields increases in the high-density region, suggesting that the compressional mode is related to the excitation of the toroidal mode. Takahashi et al. (2016) presented the radial profile of the compressional magnetic field amplitude of upstream waves observed by multi satellites during geomagnetically quiet periods. The wave amplitudes were amplified just inside the outer edge of the plasmasphere at  $L = 8$  and  $N_{e,Arase} \sim 1 \text{ cm}^{-3}$ , and such enhancement of wave power was continuously observed down to  $L = 5$  ( $N_{e,Arase} \sim 300 \text{ cm}^{-3}$ ). Because of the differences in satellite locations and highly variable amplitudes, they could not conclude that the amplification is attributed to the plasmaspheric cavity mode. From the statistical result of the wave amplitude of the toroidal and compressional mode waves, we also suggest that there may be an amplification mechanism of the upstream wave oscillations inside the plasmasphere or at the plasmopause.

The upstream wave may be a monochromatic source which is determined by the magnitude of the IMF (Equation 1); however, if the source waves penetrate the magnetosphere from multiple points and at multiple timing, the broadening of the wave spectra will occur as suggested by Takahashi, Teresawa et al. (1984). Besides the effect of multipoint wave sources, perturbations in the direction of the wave number vector and reflected ion beam at the bow shock may cause the broadening according to the theoretical prediction of upstream wave frequency (Takahashi, Teresawa et al., 1984).

### 4.3. Solar Wind Dynamic Pressure Fluctuations

This study has shown that the fluctuation of the solar wind dynamic pressure is one of the possible energy sources of MTWs. Claudepierre et al. (2010, 2016) performed global MHD simulations to investigate the field line resonance driven by the fluctuations of the solar wind dynamic pressure. They continuously imposed solar wind dynamic pressure fluctuations with broadband frequency spectra in a frequency range of 0–25 mHz at the upstream region of  $x = 20 R_E$ . In their results, the power spectral density of standing Alfvén waves was enhanced in the same frequency range of the input fluctuations. In our result, however, the broadness of the fluctuations of the solar wind dynamic pressure does not well correspond to the maximum frequency of MTWs (Figure 5a) like the simulations of Claudepierre et al. (2010, 2016). This tendency did not change when we changed the limitation of the data used for the analysis from  $N_{e,Arase} < 50 \text{ cm}^{-3}$  to  $N_{e,Arase} > 50 \text{ cm}^{-3}$ , or a specified L-shell of  $L = 6\text{--}7$ . The L-shell dependence of  $f_{\max}$  (Figure 5b) may correspond to the excitation of toroidal standing Alfvén waves by an impulse simulated by Lee and Lysak (1999) rather than the continuous input of the broadband fluctuations in Claudepierre et al. (2010, 2016). This implies that the highest frequency of MTWs is determined by the harmonics of the field line resonance rather than the frequency of source waves. The mechanism which determines the upper limit of the harmonics of standing Alfvén waves is unclear at present. In a numerical simulation of Lee and Lysak (1999), the latitudinal structure of the source wave determines the symmetric/asymmetric structure of field line oscillations. Therefore, the complexity of the latitudinal structure of the source wave is possibly responsible for the upper limit of the wave harmonics. Recently, Seki et al. (2014) performed a drift-kinetic simulation and found that the higher harmonics of input monochromatic waves appear in the case of high plasma beta. Wave-particle interaction is also possibly important for the excitation of multi-harmonic waves, and it should be investigated in a future study.

It should be noted that the dynamic pressure fluctuations can be positively correlated with the magnitude of the dynamic pressure. When the dynamic pressure of the solar wind is large, the location of the magnetopause becomes close to the Earth, resulting in a large wave power of ULF waves in the magnetosphere (Takahashi & Ukhorskiy, 2007). To discuss the effect of the magnetopause location, we conducted the statistical analysis of the

occurrence rate of MTWs under  $P_{\text{WIND}} > 5$  nPa. We obtained an occurrence rate almost the same with Figure 5, indicating only the fluctuations of the dynamic pressure are important for the excitation of MTWs.

#### 4.4. Power-Law Index $\alpha$ in the Calculation of Eigenmode Frequency

In this study, we assumed the power-law index of  $\alpha = 0.5$  for simplicity and comparison of the result with Takahashi and Denton (2021), but it is considered that the value of  $\alpha$  increases or that  $\alpha$  cannot be fixed at a single value in a low-density region (e.g., Denton et al., 2002; Goldstein et al., 2001; Takahashi & Denton, 2004). The  $\alpha$  dependence of the modeled eigenfrequency may affect the detection of a spectral peak because we selected a spectral peak that has the maximal value in the frequency range of  $\pm 30\%$  of an interval of the model frequencies.

To confirm the dependence of the model frequency on  $\alpha$ , we statistically compared the model frequencies for  $\alpha = 0.5$  ( $f_{\alpha(0.5)}^{\text{model}}$ ) and  $\alpha = 2.0$  ( $f_{\alpha(2.0)}^{\text{model}}$ ) from 23 March 2017 to 30 September 2020. We found that the ratio of  $f_{\alpha(0.5)}^{\text{model}}/f_{\alpha(2.0)}^{\text{model}}$  is strongly dependent on the magnetic latitude while the L-shell dependence is weak. The ratio ranges from  $\sim 0.7$  to 1.1 and the most frequent value is  $\sim 0.9$  for the fundamental mode. The ratio becomes significantly small ( $< 0.8$ ) at  $|\text{MLAT}| > \sim 30^\circ$  but the ratio of the data in which  $f_{\alpha(0.5)}^{\text{model}} < 0.8f_{\alpha(2.0)}^{\text{model}}$  is less than 10% of all data. Therefore, we consider that the difference of  $\alpha$  is not influential in our statistical result.

If the realistic value of  $\alpha$  is  $\sim 2$ , the shift of the peaks of observation time by  $\lesssim 10\%$  to the right of the modeled eigenfrequencies ( $f_{T1}^{\text{model}} - f_{T4}^{\text{model}}$ ) in Figure 7 can be interpreted as an effect of  $\alpha$ . Although the investigation of realistic  $\alpha$  is an important issue, strict estimation of  $\alpha$  (e.g., Obana et al., 2021) is beyond the scope of this study.

## 5. Conclusions

In this study, we have analyzed 3.5-year data of the Arase satellite and solar wind data provided by OMNIWeb and the WIND satellite to reveal the statistical relation between the multi-harmonic toroidal ULF waves and the solar wind parameters. Solar wind dependence of the occurrence rate, the wave power, and the wave frequency of the multi-harmonic toroidal waves have been examined. We have investigated the influence of local plasma density at the spacecraft position on wave excitation. The results of our analysis are summarized as follows:

1. The occurrence and wave power of the multi-harmonic toroidal waves exhibit MLT dependence on the solar wind velocity and the cone angle of the IMF. The occurrence rate and the wave power on the flank sides increase with the solar wind speed. In the noon sector (09–15 MLT), the occurrence rate and the median value of the harmonic wave frequencies exhibit positive correlations with the cone angle
2. The occurrence rate of the multi-harmonic toroidal waves increases with the power spectral density of the solar wind dynamic pressure fluctuations for a low-speed solar wind condition ( $V_{\text{sw}} < 450$  km/s). The broadness of the power spectral density of the solar wind dynamic pressure fluctuations is not strongly associated with the maximum frequency of the multi-harmonic toroidal waves
3. The occurrence frequency of the multi-harmonic toroidal waves increases when the spacecraft is located in the extremely low-density region ( $N_{e,\text{Arase}} \lesssim 1$  cm $^{-3}$ ) or inside the plasmasphere ( $N_{e,\text{Arase}} \gtrsim 100$  cm $^{-3}$ )
4. The maximum frequency of the multi-harmonic waves is proportional to the interval of the eigenfrequencies of toroidal standing Alfvén waves

From these results, we suggest that the KH instability and the solar wind dynamic pressure fluctuations are also the energy sources of the multi-harmonic toroidal waves as well as the cone angle. We consider that the KH instability is related to the multi-harmonic waves with large amplitudes on the flank sides and that the cone angle and dynamic pressure fluctuations are related to the waves around noon. However, we note that multiple energy sources are possible for an observation of the multi-harmonic toroidal waves. Local electron density may play an important role in the occurrence of the multi-harmonic toroidal waves. We propose two scenarios of the occurrence of the multi-harmonic toroidal waves related to the high electron density region: the effect of narrow spacing of eigenmode frequencies of standing Alfvén waves and the mode coupling in the plasmasphere.

Our statistical study has resolved the complicated solar wind condition into several simple situations to study the solar wind dependence of the occurrence rate, the wave power, and the frequency of the multi-harmonic toroidal waves for the first time. This study proposes that various kinds of energy sources of ULF waves can excite the multi-harmonic toroidal waves. As indicated by the previous numerical study (Sarris et al., 2017), these waves

may affect the dynamics of radiation belt electrons in a wide energy range. Further analysis of the relation between the multi-harmonic/broadband ULF waves and the energy spectra of the relativistic electrons is needed in the future.

## Data Availability Statement

Science data of the ERG (Arase) satellite were obtained from the ERG Science Center operated by ISAS/JAXA and ISEE/Nagoya University (<https://ergsc.isee.nagoya-u.ac.jp/index.shtml.en>, Miyoshi, Hori et al., 2018). The Arase satellite data sets used in this study are available in these in-text data citation references: Matsuoka, Teramoto, Imajo, et al., (2018), Kasahara et al. (2021), and Miyoshi, Shinora & Jun, (2018). In the present study, MGF Lv.2 64-Hz data v03\_04 and electron density Lv.3 v01\_01 data of PWE/HFA were used. The high-resolution solar wind data are obtained from OMNIWeb (<https://omniweb.gsfc.nasa.gov/>). The plasma data of the WIND satellite are available at CDAWeb (<https://cdaweb.gsfc.nasa.gov/pub/data/wind/3dp/>).

## References

### Acknowledgments

K. Yamamoto is supported by Grand-in-Aid for Research Fellow of Japan Society for the Promotion of Science (JSPS) (21J00921). K. Seki is supported by Grant-in-Aid for Specially Promoted Research (16H06286) and Grant-in-Aid for Scientific Research (A) (20H00192). S. Imajo is supported by JSPS Grand-in-Aid for Young Scientists (21K13977) and the Chubei Itoh Foundation. M. Teramoto is supported by Grant-in-Aid for Scientific Research (C) (19K03948). I. Shinohara is supported by Grant-in-Aid for Scientific Research (S) (17H06140).

- Anderson, B. J., & Engebretson, M. J. (1995). Relative intensity of toroidal and compressional Pc 3–4 wave power in the dayside outer magnetosphere. *Journal of Geophysical Research*, *100*(A6), 9591–9603. <https://doi.org/10.1029/95JA00132>
- Anderson, B. J., Engebretson, M. J., Rounds, S. P., Zanetti, L. J., & Potemra, T. A. (1990). A statistical study of Pc 3–5 pulsations observed by the AMPTE/CCE magnetic fields experiment. I. Occurrence distributions. *Journal of Geophysical Research*, *95*(A7), 10495–10523. <https://doi.org/10.1029/JA095iA07p10495>
- Cao, M., McPherron, R. L., & Russell, C. T. (1994). Statistical study of ULF wave occurrence in the dayside magnetosphere. *Journal of Geophysical Research*, *99*, 8731–8753. <https://doi.org/10.1029/93JA02905>
- Claudepierre, S. G., Elkington, S. R., & Wiltberger, M. (2008). Solar wind driving of magnetospheric ULF waves: Pulsations driven by velocity shear at the magnetopause. *Journal of Geophysical Research*, *113*, A05218. <https://doi.org/10.1029/2007JA012890>
- Claudepierre, S. G., Hudson, M. K., Lotko, W., Lyon, J. G., & Denton, R. E. (2010). Solar wind driving of magnetospheric ULF waves: Field line resonances driven by dynamic pressure fluctuations. *Journal of Geophysical Research*, *115*, A11202. <https://doi.org/10.1029/2010JA015399>
- Claudepierre, S. G., Mann, I. R., Takahashi, K., Fennell, J. F., Hudson, M. K., Blake, J. B., et al. (2013). Van Allen Probes observation of localized drift resonance between poloidal mode ultra-low frequency waves and 60 keV electrons. *Geophysical Research Letters*, *40*, 4491–4497. <https://doi.org/10.1002/grl.50901>
- Claudepierre, S. G., Toffoletto, F. R., & Wiltberger, M. (2016). Global MHD modeling of resonant ULF waves: Simulations with and without a plasmasphere. *Journal of Geophysical Research: Space Physics*, *121*, 227–244. <https://doi.org/10.1002/2015JA022048>
- Denton, R. E., Goldstein, J., Menietti, J. D., & Young, S. L. (2002). Magnetospheric electron density model inferred from Polar plasma wave data. *Journal of Geophysical Research*, *107*(A11), 1386. <https://doi.org/10.1029/2001JA009136>
- Elkington, S. R., Hudson, M. K., & Chan, A. A. (1999). Acceleration of relativistic electrons via drift-resonant interaction with toroidal-mode Pc-5 ULF oscillations. *Geophysical Research Letters*, *26*(21), 3273–3276. <https://doi.org/10.1029/1999gl003659>
- Engebretson, M. J., Zanetti, L. J., Potemra, T. A., & Acuna, M. H. (1986). Harmonically structured ULF pulsations observed by the AMPTE CCE magnetic field experiment. *Geophysical Research Letters*, *13*(9), 905–908. <https://doi.org/10.1029/gl013i009p00905>
- Engebretson, M. J., Zanetti, L. J., Potemra, T. A., Baumjohann, W., Lühr, H., & Acuna, M. H. (1987). Simultaneous observation of Pc 3–4 pulsations in the solar wind and in the Earth's magnetosphere. *Journal of Geophysical Research*, *92*(A9), 10053–10062. <https://doi.org/10.1029/JA092iA09p10053>
- Fairfield, D. H. (1969). Bow shock associated waves observed in the far upstream interplanetary medium. *Journal of Geophysical Research*, *74*(14), 3541–3553. <https://doi.org/10.1029/JA074i014p03541>
- Fei, Y., Chan, A. A., Elkington, S. R., & Wiltberger, M. J. (2006). Radial diffusion and MHD particle simulations of relativistic electron transport by ULF waves in the September 1998 storm. *Journal of Geophysical Research*, *111*, A12209. <https://doi.org/10.1029/2005JA011211>
- Goldstein, J., Denton, R. E., Hudson, M. K., Miftakhova, E. G., Young, S. L., Menietti, J. D., & Gallagher, D. L. (2001). Latitudinal density dependence of magnetic field lines inferred from Polar plasma wave data. *Journal of Geophysical Research*, *106*(A4), 6195–6201. <https://doi.org/10.1029/2000JA000068>
- Gupta, J. C. (1975). Long-period Pc5 pulsations. *Planetary and Space Science*, *23*, 733–750. [https://doi.org/10.1016/0032-0633\(75\)90012-4](https://doi.org/10.1016/0032-0633(75)90012-4)
- He, F., Zhang, X.-X., Lin, R.-L., Fok, M.-C., Katus, R. M., Liemohn, M. W., et al. (2017). A new solar wind-driven global dynamic plasmapause model: 2. Model and validation. *Journal of Geophysical Research: Space Physics*, *122*, 7172–7187. <https://doi.org/10.1002/2017JA023913>
- Heilig, B., Lühr, H., & Rother, M. (2007). Comprehensive study of ULF upstream waves observed in the topside ionosphere by CHAMP and on the ground. In *Annales geophysicae*, (Vol. 25(3), Copernicus GmbH, pp. 737–754. <https://doi.org/10.5194/angeo-25-737-2007>
- Horwitz, J. L., Comfort, R. H., & Chappell, C. R. (1984). Thermal ion composition measurements of the formation of the new outer plasmasphere and double plasmapause during storm recovery phase. *Geophysical Research Letters*, *11*, 701–704. <https://doi.org/10.1029/GL011i008p00701>
- Imajo, S., Miyoshi, Y., Kazama, Y., Asamura, K., Shinohara, I., Shiokawa, K., et al. (2021). Active auroral arc powered by accelerated electrons from very high altitudes. *Scientific Reports*, *11*, 1610. <https://doi.org/10.1038/s41598-020-79665-5>
- Inglis, A. R., Ireland, J., Dennis, B. R., Hayes, L., & Gallagher, P. (2016). A large-scale search for evidence of quasi-periodic pulsations in solar flares. *The Astrophysical Journal*, *833*(2), 284. <https://doi.org/10.3847/1538-4357/833/2/284>
- Inglis, A. R., Ireland, J., & Dominique, M. (2015). Quasi-periodic pulsations in solar and stellar flares: Re-evaluating their nature in the context of power-law flare Fourier spectra. *The Astrophysical Journal*, *798*(2), 108. <https://doi.org/10.1088/0004-637x/798/2/108>
- Kamiya, K., Seki, K., Saito, S., Amano, T., & Miyoshi, Y. (2018). Formation of butterfly pitch angle distributions of relativistic electrons in the outer radiation belt with a monochromatic Pc5 wave. *Journal of Geophysical Research*, *123*, 4679–4691. <https://doi.org/10.1002/2017JA024764>
- Kanekal, S., & Miyoshi, Y. (2021). Dynamics of the terrestrial radiation belts: A review of recent results during the VarSITI (variability of the Sun and its terrestrial impact) era, 2014–2018. *Progress in Earth and Planetary Science*, *8*, 35. <https://doi.org/10.1186/s40645-021-00413-y>
- Kasahara, Y., Kumamoto, A., Tsuchiya, F., Kojima, H., Matsuda, S., Matsuoka, A., et al. (2021). The PWE/HFA instrument level-3 electron density data of Exploration of Energization and Radiation in Geospace (ERG) Arase satellite. <https://doi.org/10.34515/DATA>



- Keiling, A., Wygant, J. R., Cattell, C., Kim, K.-H., Russell, C. T., Milling, D. K., et al. (2001). Pi2 pulsations observed with the Polar satellite and ground stations: Coupling of trapped and propagating fast mode waves to a midlatitude field line resonance. *Journal of Geophysical Research*, *106*(A11), 25891–25904. <https://doi.org/10.1029/2001JA900082>
- Kepko, L., Spence, H. E., & Singer, H. J. (2002). ULF waves in the solar wind as direct drivers of magnetospheric pulsations. *Geophysical Research Letters*, *29*(8), 391–394. <https://doi.org/10.1029/2001GL014405>
- Kumamoto, A., Tsuchiya, F., Kasahara, Y., Kasaba, Y., Kojima, H., Yagitani, S., et al. (2018). High Frequency Analyzer (HFA) of Plasma Wave Experiment (PWE) onboard the Arase spacecraft. *Earth Planets and Space*, *70*, 82. <https://doi.org/10.1186/s40623-018-0854-0>
- Larsen, B. A., Klumpp, D. M., & Gurgiolo, C. (2007). Correlation between plasmopause position and solar wind parameters. *Journal of Atmospheric and Solar-Terrestrial Physics*, *69*(3), 334–340. <https://doi.org/10.1016/j.jastp.2006.06.017>
- Lee, D.-H., & Lysak, R. L. (1991). Monochromatic ULF wave excitation in the dipole magnetosphere. *Journal of Geophysical Research*, *96*(A4), 5811–5817. <https://doi.org/10.1029/90JA01592>
- Lee, D.-H., & Lysak, R. L. (1999). MHD waves in a three-dimensional dipolar magnetic field: A search for Pi2 pulsations. *Journal of Geophysical Research*, *104*(A12), 28691–28699. <https://doi.org/10.1029/1999JA900377>
- Lin, R. P., Anderson, K. A., Ashford, S., Carlson, C., Curtis, D., Ergun, R., & Paschmann, G. (1995). A three-dimensional plasma and energetic particle investigation for the Wind spacecraft. *Space Science Reviews*, *71*(1–4), 125–153. <https://doi.org/10.1007/bf00751328>
- Liu, W., Sarris, T. E., Li, X., Elkington, S. R., Ergun, R., Angelopoulos, V., et al. (2009). Electric and magnetic field observations of Pc4 and Pc5 pulsations in the inner magnetosphere: A statistical study. *Journal of Geophysical Research*, *114*, A12206. <https://doi.org/10.1029/2009JA014243>
- Mathie, R. A., & Mann, I. R. (2001). On the solar wind control of Pc5 ULF pulsation power at mid-latitudes: Implications for MeV electron acceleration in the outer radiation belt. *Journal of Geophysical Research*, *106*(A12), 29783–29796. <https://doi.org/10.1029/2001JA000002>
- Matsui, H., Puhl-Quinn, P. A., Torbert, R. B., Baumjohann, W., Farrugia, C. J., Mouikis, C. G., et al. (2007). Cluster observations of broadband ULF waves near the dayside polar cap boundary: Two detailed multi-instrument event studies. *Journal of Geophysical Research*, *112*, A07218. <https://doi.org/10.1029/2007JA012251>
- Matsuoka, A., Teramoto, M., Imajo, S., Kurita, S., Miyoshi, Y., & Shinohara, I. (2018). The MGF instrument Level-2 spin-averaged magnetic field data of Exploration of energization and Radiation in Geospace (ERG) Arase satellite. ERG-06001. <https://doi.org/10.34515/DATA>
- Matsuoka, A., Teramoto, M., Nomura, R., Nosé, M., Fujimoto, A., Tanaka, Y., et al. (2018). The ARASE (ERG) magnetic field investigation. *Earth Planets and Space*, *70*, 43. <https://doi.org/10.1186/s40623-018-0800-1>
- McIlwain, C. E. (1961). Coordinates for mapping the distribution of magnetically trapped particles. *Journal of Geophysical Research*, *66*(11), 3681–3691. <https://doi.org/10.1029/JZ066011p03681>
- Miyoshi, Y., Hori, T., Shoji, M., Teramoto, M., Chang, T. F., Matsuda, S., et al. (2018). The ERG science center. *Earth Planets and Space*, *70*. <https://doi.org/10.1186/s40623-018-0867-8>
- Miyoshi, Y., Shinohara, I., & Jun, C.-W. (2018). The level-2 orbit data of Exploration of energization and Radiation in Geospace (ERG) Arase satellite, version v03. ERG Science Center, Institute for Space-Earth Environmental Research, Nagoya University. updated daily. <https://doi.org/10.34515/DATA>
- Miyoshi, Y., Shinohara, I., Takashima, T., Asamura, K., Higashio, N., Mitani, T., et al. (2018). Geospace exploration project ERG. *Earth Planets and Space*, *70*, 101. <https://doi.org/10.1186/s40623-018-0862-0>
- Murphy, K. R., Inglis, A. R., Sibeck, D. G., Watt, C. E. J., & Rae, I. J. (2020). Inner magnetospheric ULF waves: The occurrence and distribution of broadband and discrete wave activity. *Journal of Geophysical Research: Space Physics*, *125*, e2020JA027887. <https://doi.org/10.1029/2020JA027887>
- Nosé, M., Iyemori, T., Sugiura, M., & Slavin, J. A. (1995). A strong dawn/dusk asymmetry in Pc5 pulsation occurrence observed by the DE-1 satellite. *Geophysical Research Letters*, *22*(15), 2053–2056. <https://doi.org/10.1029/95GL01794>
- Nosé, M., Oimatsu, S., Keika, K., Kletzing, C. A., Kurth, W. S., Pascale, S. D., et al. (2015). Formation of the oxygen torus in the inner magnetosphere: Van Allen Probes observations. *Journal of Geophysical Research: Space Physics*, *120*, 1182–1196. <https://doi.org/10.1002/2014JA020593>
- Obana, Y., Miyashita, Y., Maruyama, N., Shinbori, A., Nose, M., Shoji, M., et al. (2021). Field-aligned electron density distribution of the inner magnetosphere inferred from coordinated observations of Arase and Van Allen Probes. *Journal of Geophysical Research*, *126*, e2020JA029073. <https://doi.org/10.1029/2020JA029073>
- Odera, T. J., Van Swol, D., Russell, C. T., & Green, C. A. (1991). Pc 3, 4 magnetic pulsations observed simultaneously in the magnetosphere and at multiple ground stations. *Geophysical Research Letters*, *18*(9), 1671–1674. <https://doi.org/10.1029/91GL01297>
- Olson, J. V., & Rostoker, G. (1978). Longitudinal phase variations of Pc 4–5 micropulsations. *Journal of Geophysical Research*, *83*(A6), 2481–2488. <https://doi.org/10.1029/JA083iA06p02481>
- Ozeke, L. G., Mann, I. R., Murphy, K. R., Jonathan Rae, I., & Milling, D. K. (2014). Analytic expressions for ULF wave radiation belt radial diffusion coefficients. *Journal of Geophysical Research: Space Physics*, *119*, 1587–1605. <https://doi.org/10.1002/2013JA019204>
- Ozeke, L. G., Mann, I. R., Murphy, K. R., Rae, I. J., Milling, D. K., Elkington, S. R., et al. (2012). ULF wave derived radiation belt radial diffusion coefficients. *Journal of Geophysical Research*, *117*, A04222. <https://doi.org/10.1029/2011JA017463>
- Ponomarenko, P. V., Waters, C. L., Sciffer, M. D., Fraser, B. J., & Samson, J. C. (2001). Spatial structure of ULF waves: Comparison of magnetometer and super dual auroral radar network data. *Journal of Geophysical Research*, *106*(A6), 10509–10517. <https://doi.org/10.1029/2000JA000281>
- Sarris, T. E. (2014). Estimates of the power per mode number of broadband ULF waves at geosynchronous orbit. *Journal of Geophysical Research: Space Physics*, *119*, 5539–5550. <https://doi.org/10.1002/2013JA019238>
- Sarris, T. E., Li, X., Liu, W., Argyriadis, E., Boudouridis, A., & Ergun, R. (2013). Mode number calculations of ULF field-line resonances using ground magnetometers and THEMIS measurements. *Journal of Geophysical Research: Space Physics*, *118*, 6986–6997. <https://doi.org/10.1002/2012JA018307>
- Sarris, T. E., Li, X., Temerin, M., Zhao, H., Califf, S., Liu, W., & Ergun, R. (2017). On the relationship between electron flux oscillations and ULF wave-driven radial transport. *Journal of Geophysical Research: Space Physics*, *122*, 9306–9319. <https://doi.org/10.1002/2016JA023741>
- Sarris, T. E., Liu, W., Kabin, K., Li, X., Elkington, S. R., Ergun, R., et al. (2009). Characterization of ULF pulsations by THEMIS. *Geophysical Research Letters*, *36*, L04104. <https://doi.org/10.1029/2008GL036732>
- Schulz, M., & Lanzerotti, L. J. (1974). Pitch-angle diffusion. In *Particle diffusion in the radiation belts. Physics and Chemistry in Space* (Vol. 7). Springer. [https://doi.org/10.1007/978-3-642-65675-0\\_3](https://doi.org/10.1007/978-3-642-65675-0_3)
- Schwarz, G. (1978). Estimating the dimension of a model. *Annals of Statistics*, *6*(2), 461–464.
- Seki, K., Amano, T., Saito, S., Miyoshi, Y., Matsumoto, Y., Umeda, T., & Miyashita, Y. (2014). A study on characteristics of radial transport of relativistic electrons by ULF Pc5 waves in the inner magnetosphere based on the GEMSIS-RC and RB models. In *AGU Fall Meeting Abstracts* (Vol. 2014, pp. SM43B–4301).

- Shi, X., Hartinger, M. D., Baker, J. B. H., Ruohoniemi, J. M., Lin, D., Xu, Z., et al. (2020). Multipoint conjugate observations of dayside ULF waves during an extended period of radial IMF. *Journal of Geophysical Research: Space Physics*, *125*, e2020JA028364. <https://doi.org/10.1029/2020JA028364>
- Singer, H. J., Russell, C. T., Kivelson, M. G., Greenstadt, E. W., & Olson, J. V. (1977). Evidence for the control of Pc 3,4 magnetic pulsations by the solar wind velocity. *Geophysical Research Letters*, *4*, 377–379. <https://doi.org/10.1029/GL004i009p00377>
- Singer, H. J., Southwood, D. J., Walker, R. J., & Kivelson, M. G. (1981). Alfvén wave resonances in a realistic magnetospheric magnetic field geometry. *Journal of Geophysical Research*, *86*(A6), 4589–4596. <https://doi.org/10.1029/JA086iA06p04589>
- Southwood, D. J., Dungey, J. W., & Etherington, R. J. (1969). Bounce resonant interaction between pulsations and trapped particles. *Planetary and Space Science*, *17*(3), 349–361.
- Takahashi, K., Anderson, B. J., & Ohtani, S. (1996). Multisatellite study of nightside transient toroidal waves. *Journal of Geophysical Research*, *101*(A11), 24815–24825. <https://doi.org/10.1029/96JA02045>
- Takahashi, K., Bonnell, J., Glassmeier, K.-H., Angelopoulos, V., Singer, H. J., Chi, P. J., et al. (2010). Multipoint observation of fast mode waves trapped in the dayside plasmasphere. *Journal of Geophysical Research*, *115*, A12247. <https://doi.org/10.1029/2010JA015956>
- Takahashi, K., & Denton, R. E. (2021). Nodal structure of toroidal standing Alfvén waves and its implication for field line mass density distribution. *Journal of Geophysical Research: Space Physics*, *126*, e2020JA028981. <https://doi.org/10.1029/2020JA028981>
- Takahashi, K., Denton, R. E., Anderson, R. R., & Hughes, W. J. (2004). Frequencies of standing Alfvén wave harmonics and their implication for plasma mass distribution along geomagnetic field lines: Statistical analysis of CRRES data. *Journal of Geophysical Research*, *109*, A08202. <https://doi.org/10.1029/2003JA010345>
- Takahashi, K., Denton, R. E., Hirahara, M., Min, K., Ohtani, S., & Sanchez, E. (2014). Solar cycle variation of plasma mass density in the outer magnetosphere: Magnetoseismic analysis of toroidal standing Alfvén waves detected by Geotail. *Journal of Geophysical Research: Space Physics*, *119*, 8338–8356. <https://doi.org/10.1002/2014JA020274>
- Takahashi, K., Denton, R. E., Kurth, W., Kletzing, C., Wygant, J., Bonnell, J., et al. (2015). Externally driven plasmaspheric ULF waves observed by the Van Allen Probes. *Journal of Geophysical Research: Space Physics*, *120*, 526–552. <https://doi.org/10.1002/2014JA020373>
- Takahashi, K., Hartinger, M. D., Angelopoulos, V., & Glassmeier, K.-H. (2015). A statistical study of fundamental toroidal mode standing Alfvén waves using THEMIS ion bulk velocity data. *Journal of Geophysical Research: Space Physics*, *120*, 6474–6495. <https://doi.org/10.1002/2015JA021207>
- Takahashi, K., Hartinger, M. D., Malaspina, D. M., Smith, C. W., Koga, K., Singer, H. J., et al. (2016). Propagation of ULF waves from the upstream region to the midnight sector of the inner magnetosphere. *Journal of Geophysical Research: Space Physics*, *121*, 8428–8447. <https://doi.org/10.1002/2016JA022958>
- Takahashi, K., McPherron, R. L., & Hughes, W. J. (1984). Multispacecraft observations of the harmonic structure of Pc 3–4 magnetic pulsations. *Journal of Geophysical Research*, *89*(A8), 6758–6774. <https://doi.org/10.1029/JA089iA08p06758>
- Takahashi, K., McPherron, R. L., & Terasawa, T. (1984). Dependence of the spectrum of Pc 3–4 pulsations on the interplanetary magnetic field. *Journal of Geophysical Research*, *89*(A5), 2770–2780. <https://doi.org/10.1029/JA089iA05p02770>
- Takahashi, K., Ohtani, S., Denton, R. E., Hughes, W. J., & Anderson, R. R. (2008). Ion composition in the plasma trough and plasma plume derived from a Combined Release and Radiation Effects Satellite magnetoseismic study. *Journal of Geophysical Research*, *113*, A12203. <https://doi.org/10.1029/2008JA013248>
- Takahashi, K., & Ukhorskiy, A. Y. (2007). Solar wind control of Pc5 pulsation power at geosynchronous orbit. *Journal of Geophysical Research*, *112*, A11205. <https://doi.org/10.1029/2007JA012483>
- Takahashi, K., Vellante, M., Del Corpo, A., Claudepierre, S. G., Kletzing, C., Wygant, J., & Koga, K. (2020). Multiharmonic toroidal standing Alfvén waves in the midnight sector observed during a geomagnetically quiet period. *Journal of Geophysical Research: Space Physics*, *125*, e2019JA027370. <https://doi.org/10.1029/2019JA027370>
- Takahashi, K., Waters, C., Glassmeier, K.-H., Kletzing, C. A., Kurth, W. S., & Smith, C. W. (2015). Multifrequency compressional magnetic field oscillations and their relation to multiharmonic toroidal mode standing Alfvén waves. *Journal of Geophysical Research: Space Physics*, *120*(10384–10), 403. <https://doi.org/10.1002/2015JA021780>
- Tan, L. C., Fung, S. F., & Shao, X. (2004). Observation of magnetospheric relativistic electrons accelerated by Pc-5 ULF waves. *Geophysical Research Letters*, *31*, L14802. <https://doi.org/10.1029/2004GL019459>
- Teramoto, M., Hori, T., Saito, S., Miyoshi, Y., Kurita, S., Higashio, N., et al. (2019). Remote detection of drift resonance between energetic electrons and ultralow frequency waves: Multisatellite coordinated observation by Arase and Van Allen Probes. *Geophysical Research Letters*, *46*, 11642–11651. <https://doi.org/10.1029/2019GL084379>
- Thébault, E., Finlay, C. C., Beggan, C. D., Alken, P., Aubert, J., Barrois, O., et al. (2015). International geomagnetic reference field: The 12th generation. *Earth Planets and Space*, *67*, 79. <https://doi.org/10.1186/s40623-015-0228-9>
- Tsyganenko, N. A. (1989). A magnetospheric magnetic field model with a warped tail current sheet. *Planetary and Space Science*, *37*, 5–20. [https://doi.org/10.1016/0032-0633\(89\)90066-4](https://doi.org/10.1016/0032-0633(89)90066-4)
- Vellante, M., Lühr, H., Zhang, T. L., Wesztergom, U., Villante, V., Lauretis, M. D., et al. (2004). Ground/satellite signatures of field line resonance: A test of theoretical predictions. *Journal of Geophysical Research*, *109*, A06210. <https://doi.org/10.1029/2004JA010392>
- Zhang, X. Y., Zong, Q. G., Wang, Y. F., Zhang, H., Xie, L., Fu, S. Y., et al. (2010). ULF waves excited by negative/positive solar wind dynamic pressure impulses at geosynchronous orbit. *Journal of Geophysical Research*, *115*, A10221. <https://doi.org/10.1029/2009JA015016>
- Zong, Q. G., Zhou, X. Z., Li, X., Song, P., Fu, S. Y., Baker, D. N., et al. (2007). Ultralow frequency modulation of energetic particles in the dayside magnetosphere. *Geophysical Research Letters*, *34*, L12105. <https://doi.org/10.1029/2007GL029915>